

REPORT DOCUMENTATION PAGEFORM APPROVED
OMB NO. 0704-0188

Public reporting burden for this collection of information is estimated to average 1 hour per response, including the time for reviewing instructions, searching existing data sources, gathering and maintaining the data needed, and completing and reviewing this collection of information. Send comments regarding this burden estimate or any other aspect of this collection of information, including suggestions for reducing this burden to Department of Defense, Washington Headquarters Services, Directorate for Information Operations and Reports (0704-0188), 1215 Jefferson Davis

1. REPORT DATE (DD-MM-YYYY) 07-12-2018		2. REPORT TYPE Presentation		3. DATES COVERED (From - To) 6/2018 - 7/2018	
4. TITLE AND SUBTITLE Modeling Reinforced Concrete Protective Construction for Impact Scenarios				5a. CONTRACT NUMBER	
				5b. GRANT NUMBER	
				5c. PROGRAM ELEMENT NUMBER	
6. AUTHOR(S) Bradley Durant Michael Oesterle Joseph Magallanes				5d. PROJECT NUMBER	
				5e. TASK NUMBER	
				5f. WORK UNIT NUMBER	
7. PERFORMING ORGANIZATION NAME(S) AND ADDRESS(ES) NAVFAC EXWC 1100 23 rd Ave. Port Hueneme, CA 93043				8. PERFORMING ORGANIZATION REPORT NUMBER PR-NAVFAC-EXWC-CI-1804	
9. SPONSORING / MONITORING AGENCY NAME(S) AND ADDRESS(ES) NAVFAC Headquarters 1322 Patterson Ave. Suite 1000 Washington Navy Yard, DC 20374-5065				10. SPONSOR / MONITOR'S ACRONYM(S) NAVFAC HQ	
				11. SPONSOR / MONITOR'S REPORT NUMBER(S)	
12. DISTRIBUTION / AVAILABILITY STATEMENT DISTRIBUTION STATEMENT A: Approved for public release; distribution is unlimited.					
13. SUPPLEMENTARY NOTES					
14. ABSTRACT The continuous improvement of analytical methods for determining the ability of reinforced concrete structures to resist blast effects is critical to the ever-evolving field of explosives safety. When considering impact loading from debris or fragments and localized structural response modes such as breach, spall, penetration, and perforation, simplified computational procedures are often insufficient to capture the complexity of the event. Because extensive live testing is often infeasible, validated high-fidelity analysis models can be utilized to capture structural response to extreme loading scenarios. With this enhanced computational capability comes the challenge of accurately modeling the mechanical properties of concrete under complex states of stress, material cracking, large deformations, and high strain rates. This paper evaluates several concrete models using the high-fidelity physics-based code LS-DYNA with respect to their ability to simulate the response of high-strength concrete to a localized impact event. Each material model was subjected to a variety of quasi-static loading patterns at the single element level as well as projectile impact loading, and the results were compared against laboratory test data. The study provides insight into the correlations between improved modeling of high-strength concrete response to quasi-static loading and the ability to simulate impact events with greater accuracy.					
15. SUBJECT TERMS Protective Construction, Physics-Based Modeling, Reinforced Concrete, Impact, Debris, Explosives Safety					
16. SECURITY CLASSIFICATION OF:			17. LIMITATION OF ABSTRACT	18. NUMBER OF PAGES	19a. NAME OF RESPONSIBLE PERSON
a. REPORT	b. ABSTRACT	c. THIS PAGE			Bradley Durant
U	U	U	U	31	19b. TELEPHONE NUMBER (include area code) 805-982-4852

This page is intentionally left blank.

Modeling Reinforced Concrete Protective Construction for Impact Scenarios

Brad Durant; NAVFAC EXWC; Port Hueneme, CA, USA

Michael Oesterle, Ph.D., P.E.; NAVFAC EXWC; Port Hueneme, CA, USA

Joseph Magallanes, P.E., S.E.; Karagozian and Case; Glendale, CA, USA

Keywords

Protective Construction, Physics-Based Modeling, Reinforced Concrete, Impact, Debris, Explosives Safety

Abstract

The continuous improvement of analytical methods for determining the ability of reinforced concrete structures to resist blast effects is critical to the ever-evolving field of explosives safety. When considering impact loading from debris or fragments and localized structural response modes such as breach, spall, penetration, and perforation, simplified computational procedures are often insufficient to capture the complexity of the event. Because extensive live testing is often infeasible, validated high-fidelity analysis models can be utilized to capture structural response to extreme loading scenarios. With this enhanced computational capability comes the challenge of accurately modeling the mechanical properties of concrete under complex states of stress, material cracking, large deformations, and high strain rates. This paper evaluates several concrete models using the high-fidelity physics-based code LS-DYNA with respect to their ability to simulate the response of high-strength concrete to a localized impact event. Each material model was subjected to a variety of quasi-static loading patterns at the single element level as well as projectile impact loading, and the results were compared against laboratory test data. The study provides insight into the correlations between improved modeling of high-strength concrete response to quasi-static loading and the ability to simulate impact events with greater accuracy.

Introduction

Analysis of reinforced concrete protective construction features for explosives safety compliance requires tried-and-true modeling techniques which ensure the safety of personnel and equipment. While accepted analytical procedures are in place and well-documented for most of the loading scenarios associated with explosives safety practice, specific hazards such as large debris impact are not explicitly included in the governing criteria documents, leaving engineers to utilize simplified conservative approaches which do not account for many of the details associated with such complex events. More advanced modeling techniques which can adequately simulate concrete structural response to localized loading can provide engineers with an additional tool to compute impact scenarios and reduce the amount of conservatism which naturally comes along with more simplified methods. This paper provides a study displaying the value of utilizing high-fidelity physics-based models for impact problems as well as words of caution to engineers when selecting material models and parameters for these types of computations.

Protective Construction for Explosives Safety Compliance

When DoD site plans cannot provide adequate separation distances between explosives operating locations and other buildings, protective construction is required to provide an acceptable level of protection to personnel and critical infrastructure from the effects of blast overpressure, fragments, debris, and thermal hazards (DoD 6055.09M 2010). Given the common scenario of large quantities of explosive materials being stored or handled in relatively small areas, reinforced concrete construction is often the only reasonable solution to provide such protection. Thus, reliable analytical methods for determining the response of reinforced concrete structural elements and systems to blast effects is critical to the field of explosives safety.

The current governing criteria for analysis of protective construction which is required to satisfy explosives safety requirements is Unified Facilities Criteria (UFC) 3-340-02 (Structures to Resist the Effects of Accidental Explosions) (DoD 2014). This document was derived from a combination of the Army TM 5-1300, Navy P-397, and Air Force AFR 88-22 criteria and has been developed by blast-resistant design experts over the course of several decades. A significant amount of live testing has been conducted to validate the analysis methods included in the criteria for the response of structures to blast effects. While the use of methods provided in UFC3-340-02 is required for analysis of protective construction features associated with explosives safety evaluations, research is ongoing to continuously improve the criteria and develop new versions of the document which provide engineers with even better tools for designing, analyzing, and promoting safe structures.

While blast loads are reasonably predictable, at least in the mid-range and far-range, impact hazards can vary significantly from site to site. Although conservative methods are in place for estimating the effects of primary fragments on concrete structures, analysis guidance for larger debris impact scenarios is not currently included in the UFC criteria and limited in other similar supporting documents. As a result, engineers often resort to the use of very conservative approaches which utilize dynamic analysis principles and spall/breach curves or other approximate solutions in the UFC in order to satisfy the criteria. In many cases, the implications of using such an approach may not have any effect on the resulting structural requirements, particularly in cases where blast overpressure or primary fragments govern the design. However, experience has shown that this is not always the case and will not always be the case in the future.

A real-world case study provides a clear example of the type of scenario involving large debris impact and UFC compliance requirements. In this case, the quantity of Net Explosive Weight (NEW) in an ordnance assembly building had to be limited based on large-debris impact loading of a reinforced concrete structure. Analysis showed that an accidental explosion in the assembly building would result in failure of steel beam-column connections and airborne roof beams. Trajectory analysis showed that the beams could potentially impact nearby occupied concrete structures which had been shown to be acceptable for resisting overpressure and primary fragment hazards resulting from an accidental blast in the assembly building. Using a conservative approach which was derived from methods in the UFC criteria, impact analysis showed that the beam would perforate the roof of the occupied building, resulting in an unacceptable hazard and required reduction in NEW. The approach was acceptable for criteria compliance, but a more advanced analysis method would have better captured the complexity of this type of impact event, including deformation of the beam during impact and other means of energy absorption which could not be included in the simplified analysis. This paper does not include discussion of any specific advanced analysis for this case study, but it is the opinion of the authors that the roof beam hazard was significantly less severe than indicated by the conservative UFC analysis. The authors are also convinced that the use of high-fidelity physics-based modeling techniques as discussed in the remainder of this paper would likely have shown this to be true.

Given the complexity of physics-based models and level of difficulty associated with model validation and third-party review, it is understandable that the methods included in UFC 3-340-02 are strongly preferred by DoD reviewing authorities over the use of more advanced tools. However, this does not mandate that engineers cease pursuing the advancement of high-fidelity models for the purpose of explosives safety criteria compliance. The following sections will show the value of using such tools for impact scenarios involving protective construction and provide comparisons of several of the available material models for reinforced concrete.

Concrete Material Model Theoretical Background

Projectile impact into concrete involves complex states of stress, material discontinuities in the form of cracking, large material deformations, and high strain rates. Modeling these different material responses in concrete for extreme loading conditions has proven to be a significant challenge for engineers, but the continuous improvement of material models over the years has resulted in a variety of options which are worth considering. The following paragraphs provide a brief theoretical background for the modeling of concrete subjected to impact loading, with unique sections dedicated to each of the material models being investigated in this study:

- Karagozian and Case Concrete Model, Release 3 (*MAT_CONCRETE_DAMAGE_REL3)
- Continuous Surface Cap Model (*MAT_CSCM)
- Riedel-Hiermaier-Thoma Model (*MAT_RHT)

- Winfrith Concrete Model (*MAT_WINFRITH_CONCRETE)
- Johnson-Holmquist Concrete Model (*MAT_JOHNSON_HOLMQUIST_CONCRETE)
- Karagozian and Case Concrete Model, Release 4

Concrete Modeling for Impact Loading

Impact and penetration modeling of concrete structures requires a competent constitutive model for concrete, and a set of calibrated constitutive parameters for it. Important features that the constitutive model and parameters must reproduce for these problems include a strength envelope that is a function of pressure, volumetric compaction, dilatancy due to shearing, brittle and ductile material responses, and strain-rate effects, among others. Several studies already exist comparing many of the widely used models (Magallanes 2008, Wu, Crawford and Magallanes, Performance of LS-DYNA Concrete Constitutive Models 2012, Crawford, et al. 2013, Wu, Crawford and Lan, et al. 2014, Coleman 2016). In this paper, several of the concrete models available in LS-DYNA are considered.

Each of the constitutive models available in LS-DYNA are formulated using plasticity (Malvar 1997). The differences between them are subtle and manifested in how the deviatoric and volumetric responses are characterized. The response of concrete depends on pressure, and the general form of the plastic yield function is written as:

$$Y(I_1, J_2, J_3) = 0 \quad (1)$$

where I_1 is the 1st invariant of stress tensor ($I_1 = tr(\sigma_{ij})$), which represents volumetric response; J_2 and J_3 are the 2nd and 3rd invariants of deviatoric stress tensor ($\sigma_{ij} = s_{ij} + I_1 \delta_{ij} / 3, |s_{ij} - \lambda \cdot \delta_{ij}| = \lambda^3 - J_1 \lambda^2 - J_2 \lambda - J_3 = 0$).

K&C Concrete Model, Release 3

The K&C Concrete Model was first released in DYNA3D in 1994 (Malvar 1997) and was motivated by the need for response calculations for reinforced concrete structures under blast and impact effects. In MAT072_REL3, a plastic surface is derived by interpolating between two of the three independent surfaces using an internal damage variable, λ . The three surfaces denoted by $\Delta\sigma_y$, $\Delta\sigma_m$, and $\Delta\sigma_r$ represent the yield, maximum, and residual stress difference, respectively where $\Delta\sigma = \sqrt{3 \cdot J_2}$. The yield function is defined as:

$$Y(I_1, J_2, J_3, \lambda) = \sqrt{3 \cdot J_2} - \gamma(I_1, J_2, J_3, \lambda) \quad (2)$$

where

$$\gamma = \begin{cases} r(J_3) \cdot [\eta(\lambda) \cdot (\Delta\sigma_m - \Delta\sigma_y) + \Delta\sigma_y] & \lambda \leq \lambda_m \\ r(J_3) \cdot [\eta(\lambda) \cdot (\Delta\sigma_m - \Delta\sigma_r) + \Delta\sigma_r] & \lambda > \lambda_m \end{cases} \quad (3)$$

where $\eta(\lambda)$ is a nonlinear function that ranges from zero to unity for $\lambda \leq \lambda_m$ and from unity to zero when $\lambda > \lambda_m$, and λ is accumulated as a function of the effective plastic strain using three damage accumulation parameters: b_1 , b_2 , b_3 . The three surfaces are illustrated in Figure 1a, along with an arbitrary triaxial compression loading path in the pressure ($p=I_1/3$) and stress difference, $p-\Delta\sigma$, plane.

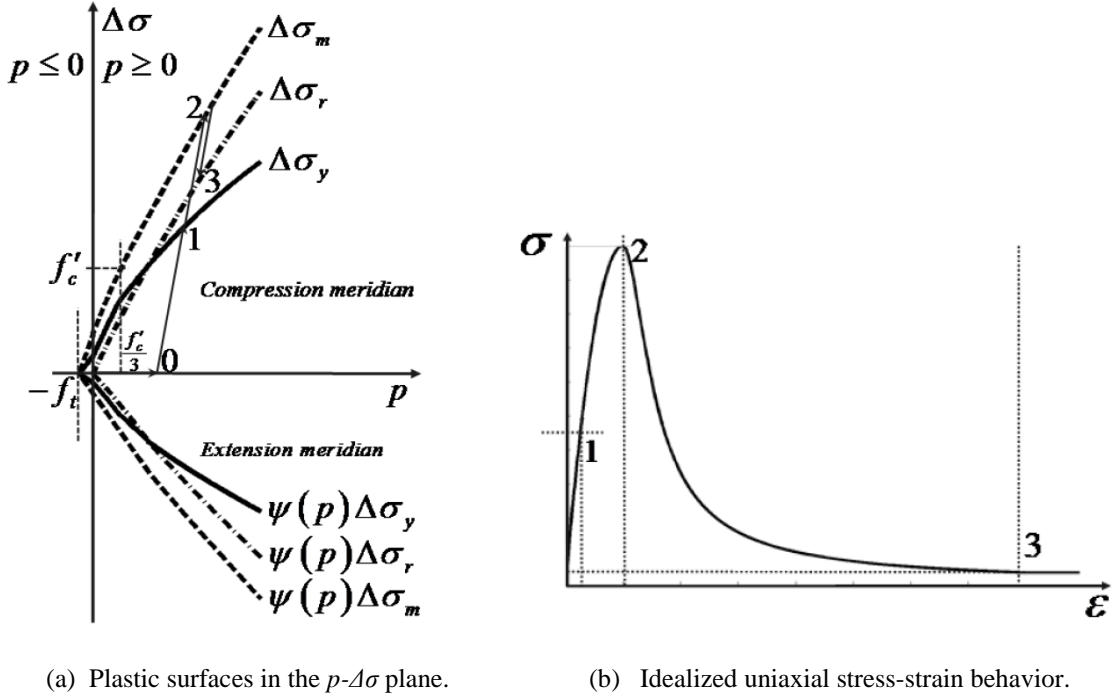


Figure 1: Illustration of the Function of the Plastic Surfaces for MAT072 REL3

The three independent surfaces, denoted here as $\Delta\sigma_i$, use a simple function to account for the effects of pressure and are calibrated to triaxial compression data. Three parameters a_{0i} , a_{1i} , and a_{2i} (9 parameters total for the three surfaces) define each of the failure surfaces:

$$\Delta\sigma_i = a_{0i} + \frac{p}{a_{1i} + a_{2i} \cdot p} \quad (4)$$

As seen in Equation (3), each of the surfaces are functions of J_3 via the function, r , using the formulation proposed by William and Warnke (Chen 1982):

$$r = \frac{2(1 - \alpha^2)\cos\theta + (2\alpha - 1\sqrt{4(1 + \alpha^2)\cos^2\theta + 5\alpha^2 - 4\alpha})}{4(1 - \alpha^2)\cos^2\theta(1 - 2\alpha)^2} \quad (5)$$

where α is a parameter that depends on pressure and the Lode angle θ can be determined from:

$$\cos 3\theta = \frac{3\sqrt{3}}{2} \frac{J_3}{J_2^{3/2}} \quad (6)$$

Strain hardening and softening behaviors are efficiently modeled by formulating the plasticity model in this way. The $\eta(\lambda)$ damage function provides the mechanism by which MAT072_REL3 may reproduce hardening until the damage is sufficient to reach surface $\Delta\sigma_m$ and then softening until $\Delta\sigma_r$ is reached. Such a feature allows modeling brittle, ductile, and brittle-to-ductile transition behaviors. Figure 1b shows an illustration of a typical axial stress (σ or σ_{11}) versus axial strain (ε or ε_{11}) response for a generic material sample subjected to loading. Subsequent to loading the material specimen hydrostatically (Point 0), sample behavior is approximately linear up to roughly 35-65% of its peak strength (Point 0 to Point 1) and then exhibits strain hardening up to the peak strength (Point 2). Strain-softening may be observed thereafter to a residual strength whose value also depends on the level of confinement (Point 3 and on). Figure 1a illustrates the functionality of Equation (3), where γ (the current yield surface) is interpolated between the yield and maximum surfaces when $\lambda \leq \lambda_m$.

For the trial stress state in the plasticity algorithm, the plastic potential function is defined as:

$$g = \sqrt{3 \cdot J_2^*} - \omega \cdot \gamma(I_1^*, J_3^*, \lambda) \quad (7)$$

where ω is a dilatancy parameter (0 for non-associative, 1 for fully associative). By defining the plastic potential function in this way, the parameter ω functions to control the macroscopic behavior of shear-induced dilatancy. Using Equation (6), one can then derive a consistency condition for the plasticity algorithm (Malvar 1997, J. E. Crawford 2011). A classic radial return algorithm is then used to correct the trial stress.

MAT072_REL3 was developed with the intent of being used in conjunction with any equation of state (EOS) model that would capture volumetric hardening, and for this reason, is a very simple and flexible model capable of modeling various types of cementitious or geological materials. Hydrostatic compression tests are typically used to obtain pressure versus volume strain pairs for the EOS. Additionally, the MAT072_REL3 incorporates rate effects via a radial rate enhancement to the plastic surface based on the effective deviatoric strain rate and the user-defined DIF curve. This provides a means to enhance strength as a function of loading rate that is easily calibrated to Split Hopkinson Pressure Bar (SHPB) data.

K&C Concrete Model, Release 4

The KCC-R4 material model was developed to extend the KCC-R3 model to more appropriately handle the quasi-brittle behaviors observed in high and ultra-high strength concretes. In the KCC-R4 formulation, a new additional internal damage variable λ_t is introduced for plastic deformation incurred under negative pressures (i.e., $p < 0$). This is done to treat the quasi-brittle behaviors observed for concrete in a more appropriate way, in addition to providing a simple extension to incorporate anisotropy from the concrete's cracking. In the version employed in these calculations, λ_t is decoupled from the compression damage, λ , leaving no interaction between the two damage variables (though the damages can be coupled with a more elaborate formulation). The plastic surface $\Gamma(p, J_3, \lambda)$ is defined by superimposing contributions from the concrete matrix and contributions from any embedded fibers. The following governs the evolution of the plastic surface for $p < 0$:

$$\Gamma(p, J_3, \lambda) = r_f \cdot \Theta(J_3) \cdot [\Gamma_m + \Gamma_f] \quad (8)$$

$$\Gamma_m = \Delta\sigma_m(p) (1 - c_{2f}) [(1 - c_0) e^{c_1 \lambda_t} + c_0] \quad (9)$$

$$\Gamma_f = \Delta\sigma_m(p) c_{2f} [(1 - c_{0f}) e^{c_{1f} \lambda_t} + c_{1f}] \quad (10)$$

where $\Delta\sigma_m(p)$ is defined as the maximum strength surface on the extension meridian of the material, which is expressed as:

$$\Delta\sigma_m = 3(f_t + p) \quad (11)$$

and where f_t is the concrete tensile strength; $\Delta\sigma_m$ is the maximum stress difference; λ_t is defined as the effective plastic strain incurred when $p < 0$ (rather than the modified plastic strain or damage used for $p > 0$); c_0 and c_1 are the material parameters controlling the strain-softening behavior of the concrete matrix; and c_{0f} , c_{1f} and c_{2f} are parameters controlling the contribution from fiber-reinforcement. For HSC, c_{0f} is zero since there is no fiber reinforcement, and the term in Equation (9) dominates the evolution of the plastic surface. The pressure cutoff is accordingly defined as:

$$p \geq -f_t \left\{ (1 - c_{2f}) [(1 - c_0) e^{c_1 \lambda_t} + c_0] + c_{2f} [(1 - c_{0f}) e^{c_{1f} \lambda_t} + c_{1f}] \right\} \quad (12)$$

Figure 2 illustrates the plastic surface defined by the KCC-R4 formulation in the region of the Rendulic plane where $p < 0$. Note that continuity of the plastic surface is enforced for $p > 0$ on both the compression and extension meridians.

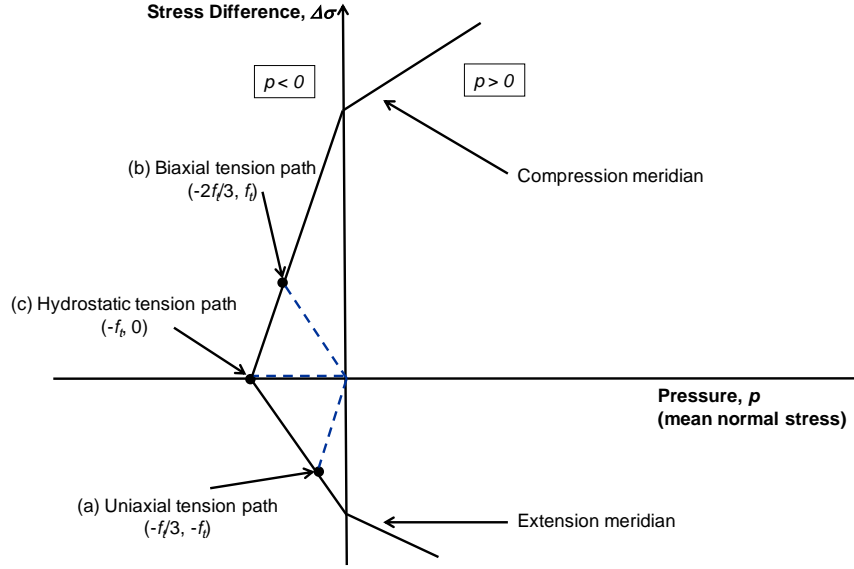


Figure 2: Plastic Surface and Resulting Behaviors Produced by the beta-KCC-R4 Material Model

Continuous Surface Cap Model

The Continuous Surface Cap model (CSCM) is an isotropic plasticity model with a damage effects and rate dependence that was developed by U.S Department of Transportation for crash and impact analysis for roadside safety applications (Federal Highway Administration, USA May 2007). This is LS-DYNA Concrete Model 159. Elastic behavior of the model is governed by the bulk modulus and the shear modulus as described by Hooke's law. Elastic behavior of the concrete remains elastic until the stress state in the concrete reaches a three dimensional yield surface at which point the concrete behaves plastically using the plastic consistency condition with an associated flow rule. The yield surface is formulated with three stress invariants and uses a multiplicative formulation to combine a shear failure surface with a hardening compaction cap surface that is smooth and continuous. The yield surface is a function of the first, second, and third stress invariants of the deviatoric stress tensor, I_1 , J'_2 , and J'_3 , respectively and κ is the hardening cap parameter as shown in the equation below:

$$Y(I_1, J'_2, J'_3, \kappa) = J'_2 - \mathfrak{R}^2 F_f^2 F_c \quad (13)$$

Where F_f is the shear failure surface, F_c is the hardening cap, and \mathfrak{R} is the Rubin third-invariant factor. The shear failure surface is defined as:

$$F_f(I_1) = \alpha - \lambda e^{-\beta I_1} + \theta I_1 \quad (14)$$

Where α , β , λ , and θ are determined by fitting the model surface to triaxial compression test data for plane concrete cylinder specimens. The cap hardening surface is defined as:

$$F_c = \begin{cases} 1 - \frac{(I_1 - L(\kappa))^2}{(X(\kappa) - L(\kappa))^2} & \text{for } I_1 \geq L(\kappa) \\ 1 & \text{for } I_1 < L(\kappa) \end{cases} \quad (15)$$

$$L(\kappa) = \begin{cases} \kappa & \kappa \geq \kappa_0 \\ \kappa_0 & \kappa \leq \kappa_0 \end{cases}$$

$$X(\kappa) = L(\kappa) + R F_f(I_1)$$

This equation describes a cap for the failure surface that occurs when I_1 is greater than or equal to $L(\kappa)$. The value of I_1 where the shear surface initially intersects with the cap surface is κ_0 . Increase in $X(\kappa)$ and κ signify expansion of the cap surface when compaction occurs, while a decrease in $X(\kappa)$ and κ signifies a contraction of the cap surface when dilation occurs. The cap moves to simulate plastic volume change. The motion of the cap is defined by the following hardening rule:

$$\varepsilon_v^P = W \left(1 - e^{D_1(X-X_0) - D_2(X-X_0)^2} \right) \quad (16)$$

where ε_v^P is the plastic volume strain, W is the maximum plastic volume strain, and R , D_1 , and D_2 are model input parameters.

Softening of the concrete in the CSCM is represented via a damage formulation. Mesh sensitivity for tensile fracture is regulated by maintaining constant fracture energy in the elements. Rate effects are accounted for using a viscoplastic formulation.

RHT Concrete Model

The Riedel-Hiermaier-Thoma (RHT) concrete model is an isotropic plasticity model with damage effects and rate dependence. The RHT model is MAT_272 in LS-DYNA. It includes capabilities to model pressure hardening, strain hardening, strain rate hardening, third invariant dependence for compressive and tensile meridians, and crack softening (Brannon August 2009, Borrvall and Riedel May 2011). Similar to the KCC and CSCM, the RHT is initial isotropic with the stress strain behavior defined by Hooke's law. Upon reaching a yield surface, the RHT model behaves plastically using an associated flow rule similar to the KCC. The RHT model also uses three failure surfaces corresponding to initial yield, maximum strength, and residual strength similar to the KCC model. The yield surface formulation for the RHT model described in (Borrvall and Riedel May 2011) uses a pressure normalized by the compressive strength and is similar to CSCM as it combines a failure surface with a cap surface. Variables shown in the following equations with * denote a parameter that is normalized by the compressive strength of the concrete. The function for the yield surface according to (Borrvall and Riedel May 2011) is given by:

$$Y(p^*, s, \dot{\varepsilon}_p, \varepsilon_p^*) = f_c \sigma_y^*(p^*, F_r(\dot{\varepsilon}_p, p^*), \varepsilon_p^*) R_3(\theta, p^*) \quad (17)$$

where R_3 is a factor calculated from the third invariant of the stress tensor and the yield function is related to the failure surface and the cap surface by:

$$\sigma_y^*(p^*, F_r, \varepsilon_p^*) = \sigma_f^* \left(\frac{p^*}{\gamma}, F_r \right) \gamma \quad (18)$$

with

$$\gamma = \varepsilon_p^* + (1 - \varepsilon_p^*) F_e F_c \quad (19)$$

The failure surface is given by:

$$\sigma_f^*(p^*, F_r) \begin{cases} A \left(p^* - \frac{F_r}{3} + \left(\frac{A}{F_r} \right)^{\frac{1}{n}} \right)^n & \text{for } 3p^* \geq F_r \\ \frac{F_r f_s^*}{Q_1} + 3p^* \left(1 - \frac{f_s^*}{Q_1} \right) & \text{for } F_r > 3p^* \geq 0 \\ \frac{F_r f_s^*}{Q_1} - 3p^* \left(\frac{1}{Q_2} - \frac{f_s^*}{Q_1 f_t^*} \right) & \text{for } 0 > 3p^* \geq 3p_t^* \\ 0 & \text{for } 3p_t^* > 3p^* \end{cases} \quad (20)$$

The elastic strength parameter, F_e , is determined by:

$$F_e = \begin{cases} g_c^* & \text{for } 3p^* \geq F_r^c g_c^* \\ g_c^* - \frac{3p^* - F_r^c g_c^*}{F_r^c g_c^* - F_r^t g_t^* f_t^*} (g_t^* - g_c^*) & \text{for } F_r^c g_c^* > 3p^* \geq F_r^t g_t^* f_t^* \\ g_t^* & \text{for } F_r^t g_t^* f_t^* > 3p^* \end{cases} \quad (21)$$

The RHT models the effect of porosity on the strength using an elliptical cap function similar to that used in the CSCM to cap the yield surface. However, the motion of the cap is dependent on the parameter α which represents the porosity using the Mie-Grunesien form of a polynomial Hugoniot and a p - α relation. The expression for this cap function provided in (Borrvall and Riedel May 2011) is shown below:

$$F_c(p^*) = \begin{cases} 1 & \text{for } p^* \leq p_c^* \\ \sqrt{1 - \left(\frac{p^* - p_c^*}{p_c^* - p_u^*}\right)^2} & \text{for } p_c^* < p^* < p_u^* \\ 0 & \text{for } p_u^* \geq X \end{cases} \quad (22)$$

where p_c^* is a pressure at which the uniaxial compressive stress path intersects the yield surface and p_u^* is the pressure where the yield surface intersects the hydrostat axis.

Rate dependence in the RHT model is handled in a similar manner to the KCC model using dynamic increase factors that scale the failure surface. Damage accumulation as a function of the total plastic strain is used to model hardening and softening in the concrete by scaling the current failure surface between yield, maximum, and residual surfaces. Mesh objectivity is enforced by maintaining a constant fracture energy similar to the implementations in the CSCM and KCC models.

Winfrith Concrete Model

The Winfrith concrete model is an isotropic plasticity model that implements the shear failure surface proposed by Ottosen (Ottosen 1977). This model is MAT_084 in LS-DYNA and is used primarily for impact simulations (Broadhouse 1995). The equation for the failure surface is provided below:

$$f(I_1, J_2, \cos 3\theta) = a \frac{J_2}{f'_c{}^2} + \xi \frac{\sqrt{J_2}}{f'_c} + b \frac{I_1}{f'_c} - 1 \quad (23)$$

where $\cos 3\theta$ is between the interval -1 to 1 and ξ is found with:

$$\xi = \begin{cases} k_1 \cos\left[\frac{1}{3} \cos^{-1}(k_2 \cos 3\theta)\right] & \text{for } \cos 3\theta \geq 0 \\ k_1 \cos\left[\frac{\pi}{3} - \frac{1}{3} \cos^{-1}(k_2 \cos 3\theta)\right] & \text{for } \cos 3\theta \leq 0 \end{cases} \quad (24)$$

where the parameter θ is the Lode angle.

The other parameters, a , b , k_1 , and k_2 are determined from uniaxial compression, uniaxial tension, biaxial compression, and triaxial compression tests.

The inclusion of the third invariant was made to consider both triaxial compression and triaxial extension. The material model also includes strain softening with regularization based on crack opening width, aggregate size, and fracture energy. Strain rate effects are included with scaling laws based on dynamic increase factors, and tensile cracking can be visualized for three orthogonal crack planes per element. Dilation of the concrete is not modeled with the flow rule.

Johnson Holmquist Concrete Model

The Johnson Holmquist Concrete Model (JHC) uses a strength model that is pressure and strain rate dependent (Holmquist and Johnson 1993) and has the following formulation:

$$\sigma^* = (A(1 - D) + BP^{*N})(1 + C \ln\left(\frac{\dot{\epsilon}}{\dot{\epsilon}_0}\right)) \quad (25)$$

where A is the cohesive strength coefficient, B is the pressure coefficient, C is the strain rate coefficient, N is the pressure exponential, D is a scalar damage variable, $\dot{\epsilon}$ is the strain rate, and $\dot{\epsilon}_0$ is a reference strain rate. The coefficients and exponential are found by fitting the model to test data. The material model behaves elastically until the stress state reaches the yield surface, at which point plastic behavior occurs assuming that the plastic flow is isochoric. The damage scaler is calculated using the following function:

$$D = \sum \frac{\Delta\epsilon_{pl} + \Delta\mu_{pl}}{\epsilon_f} \quad (26)$$

where $\Delta\mu_{pl}$ is the cumulative volumetric plastic strain caused by volumetric compaction and $\Delta\epsilon_{pl}$ is the equivalent plastic strain caused by deformation. The term ϵ_f is the plastic strain to fracture at constant pressure and is found with:

$$\epsilon_f = D1(P^* + T^*)^{D2} \quad (27)$$

where P^* and T^* are the pressure and tensile strength normalized by unconfined compressive strength and $D1$ and $D2$ are damage parameters fit with unconfined experimental data. The pressure-volume relation is defined by two equations that represent the elastic and crushing region and the locking region. The elastic and crushing region is defined by:

$$P = K_e \mu \quad (28)$$

and the locking region is defined by:

$$P = K_1\mu + K_2\mu^2 + K_3\mu^3 \quad (29)$$

where the K coefficients are material parameters fit to test data and relate to the bulk modulus.

Experimental Test Data

The experimental data was used in this study to investigate the different numerical models. The data include both quasi-static material tests and dynamic projectile impact tests of a high-strength concrete. Cylinder tests were conducted to characterize the material which was used in the impact tests and provide analysts with the critical properties which would be required for computations. The concrete was subjected to a variety of stress paths including hydrostatic compression, unconfined compression, uniaxial tension, uniaxial compression, and triaxial compression. The data acquired from each of these tests was valuable for development of a thorough understanding of the material response to various stress states and determination of the properties which are required to model concrete in a high-fidelity physics-based software tool.

Table 1 below provides a description of the cylinder tests which were conducted to support the test program and modeling efforts.

Table 1: Description of Concrete Material Characterization Tests

Test	Description
Hydrostatic Compression	Specimen is loaded with equal pressure on all faces to subject the concrete to uniform compression.
Unconfined Compression	Specimen is loaded in compression in the axial direction only and allowed to expand freely in the radial direction.
Triaxial Compression	Specimen is loaded with equal pressure on all faces, followed by loading in the axial direction while uniform pressure is held constant. The “confining pressure” partially resists expansion of the concrete in the radial direction, thus introducing a different stress state than the unconfined compression test.
Uniaxial Compression	Specimen is set in a rigid confining fixture and loaded in the axial direction only. The fixture fully resists expansion in the radial direction, thus introducing a different state of stress than either the unconfined compression or triaxial compression tests.
Uniaxial Tension (Direct Pull)	Specimen is loaded in tension in the axial direction only and allowed to deform freely in the radial direction.

Data from a series of tests involving impact of generic projectiles into reinforced high-strength concrete slabs was used in this study. These slabs were previously tested in an effort to optimize specific protective construction features and provide data points for computational model validation. Two of the tests, which were characterized by different projectile impact velocities and slab geometries, are included in this study as shown below in Table 2.

Table 2: Experimental Test Results

Test	Result
1	Projectile Perforation with Exit Velocity = 6% of Impact Velocity
2	Depth of Penetration = 97% of Slab Depth (No Perforation)

Quasi-static Single Element Simulations

The quasi-static simulations were conducted using the software tool LS-DYNA (Livermore Software Technology Corporation 2015). The ability of six different concrete material models to simulate the response of the test concrete to quasi-static loading conditions was determined by subjecting a single finite element to the following loading conditions:

- Hydrostatic compression
- Unconfined compression
- Triaxial compression with 1x confining pressure
- Triaxial compression with 4x confining pressure
- Uniaxial tension

The element was defined by a single integration point and symmetry conditions at three faces to promote greater stability in the simulation. Specific values of pressure, stress, and strain are intentionally excluded from this study, but this does not compromise the ability of the results to display valuable comparisons between material models and the test data. It is worth noting that the second case of triaxial compression included a confining pressure which was four times greater than the first case. The two triaxial cases are labeled as “1x” and “4x” in the supporting figures.

Four of the six concrete material models were selected for simulations due to their popularity among users and automatic parameter generation feature. While this feature varies slightly from model to model, the option allows the user to input only a very limited number of material properties such as the unconfined compression strength, density,

aggregate size, etc. and automatically produces all of the other necessary properties. Because many of the concrete material models have dozens of properties to input, it is not surprising that the feature is appealing to users. While use of the automatic parameter generation is sufficient for many types of problems, high-velocity impact problems involve states of stress and material failure which challenge the simplicity of the approach. The models which both include this feature and are included in the quasi-static simulation study are as follows:

- Karagozian and Case Concrete Model, Rel. 3 (*MAT_CONCRETE_DAMAGE_REL3)
- Continuous Surface Cap Model (*MAT_CSCM)
- Riedel-Hiermaier-Thoma Model (*MAT_RHT)
- Winfrith Model (*MAT_WINFRITH_CONCRETE)

It is worth noting that the Winfrith model is popular among users for a variety of dynamic problems. However, because the model is not capable of accommodating a conversion from solid (Lagrangian) elements to smoothed-particle hydrodynamics (SPH) elements, the model was not evaluated in the projectile impact portion of this study. The importance and details of the element conversion for impact simulations are discussed in the following section. Thus, the single element simulations using the Winfrith model are provided as added value to the quasi-static material model comparisons, but the model is fully omitted from all dynamic calculations in the following sections.

A more advanced approach outside of the automatic parameter generation option involves user input of each individual parameter so that the material model can be fit to the types of material test data discussed in the previous section. In particular, material failure surfaces can be better captured, which is valuable for impact problems involving large material deformation and post-yield response. While all of the models included in this study can be fit to data, only two material models were analyzed which included parameters which were specifically fit to the concrete being used in the experimental impact testing:

- Johnson-Holmquist Concrete Model (*MAT_JOHNSON_HOLMQUIST_CONCRETE)
- Karagozian and Case Concrete Model, Rel. 4

The Release 4 version of the K&C concrete model is not yet implemented in LS-DYNA but can be utilized with a user-defined material model. Some of the improvements from the Release 3 version were discussed in the theoretical background section.

As displayed in the plots below, the single element simulations (dashed lines) for all six material models were compared directly against the cylinder test data (solid black lines). To protect the data, all values of stress and strain are normalized to some critical test data point. An instability occurred in the Winfrith model in the uniaxial tension simulation, the source of which could not be easily determined. Thus, this model is excluded from this specific loading case. Also, two plots are included for the case of triaxial compression with the higher confining pressure (4x) to provide a closer look at the material models which produced a better fit to the test data.

Given the varying approaches of using either automatic parameter generation or custom fitting for different material models, the results should not be observed through the lens of simple comparison. It is reasonable to view the results of the four models utilizing automatic generation with an “apples-to-apples” approach. However, this approach is not valid for comparing the results of the automatic generation models with those of the custom fit models given that all six of the material models can be fit to data. Because the time required to produce quality fits with all models was beyond that which was allowed for this investigation, only the K&C Release 4 and Johnson-Holmquist models were pursued in this manner. In addition to being two of the more popular models for impact simulations by advanced LS-DYNA users, both models were partially fit to the material data prior to the start of the investigation, making them top candidates for the study. Whether the material parameters are automatically generated or defined by the user, all of the simulation responses shown below are valuable when studied in conjunction with the projectile impact results for each model in the following section.

A few specific loading cases show fits to the data by models using the automatic parameter generation which are just as good as or better than custom fits for the K&C Release 4 and Johnson-Holmquist models. Examples include the RHT fit to the hydrostatic compression curve and K&C Release 3 fit to the unconfined compression and direct pull

curves. However, the K&C Release 4 and Johnson-Holmquist models produce better overall fits when observing all of the material test data collectively, as expected.

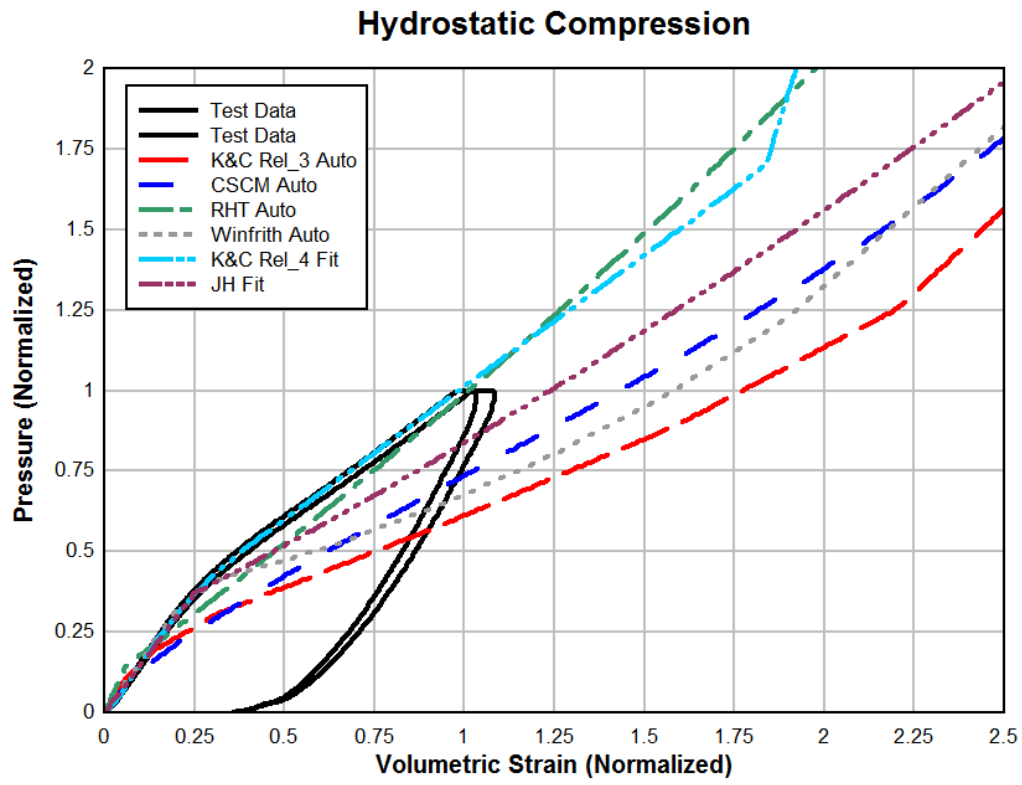


Figure 3: Hydrostatic Compression Material Test vs. Simulation Results

Unconfined Compression

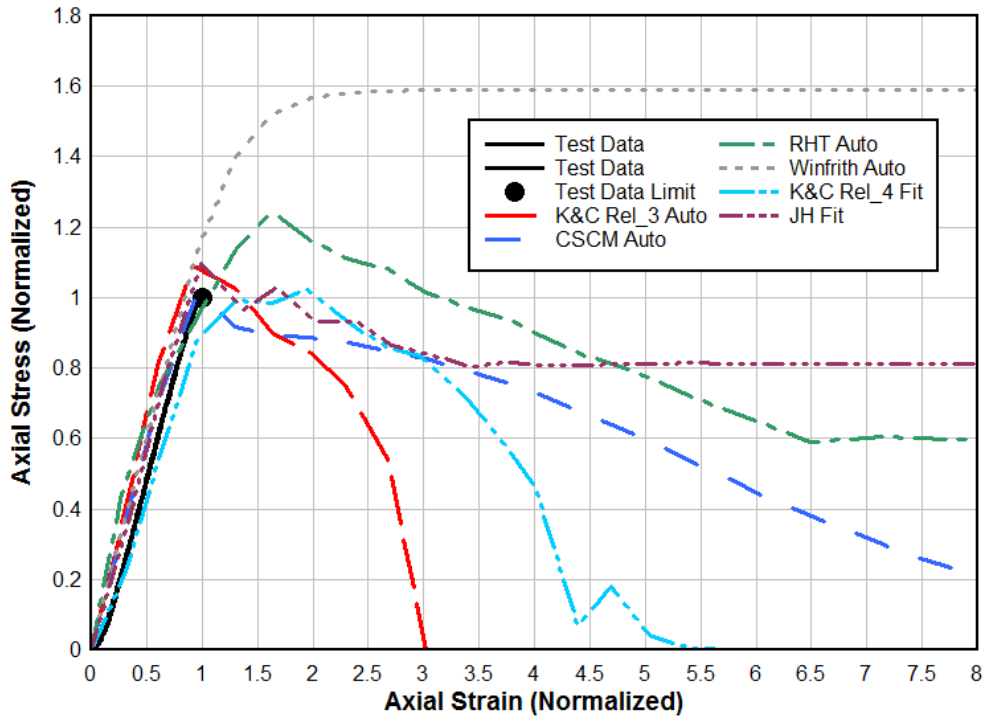


Figure 4: Unconfined Compression Material Test vs. Simulation Results

Triaxial Compression with 1x Confining Pressure

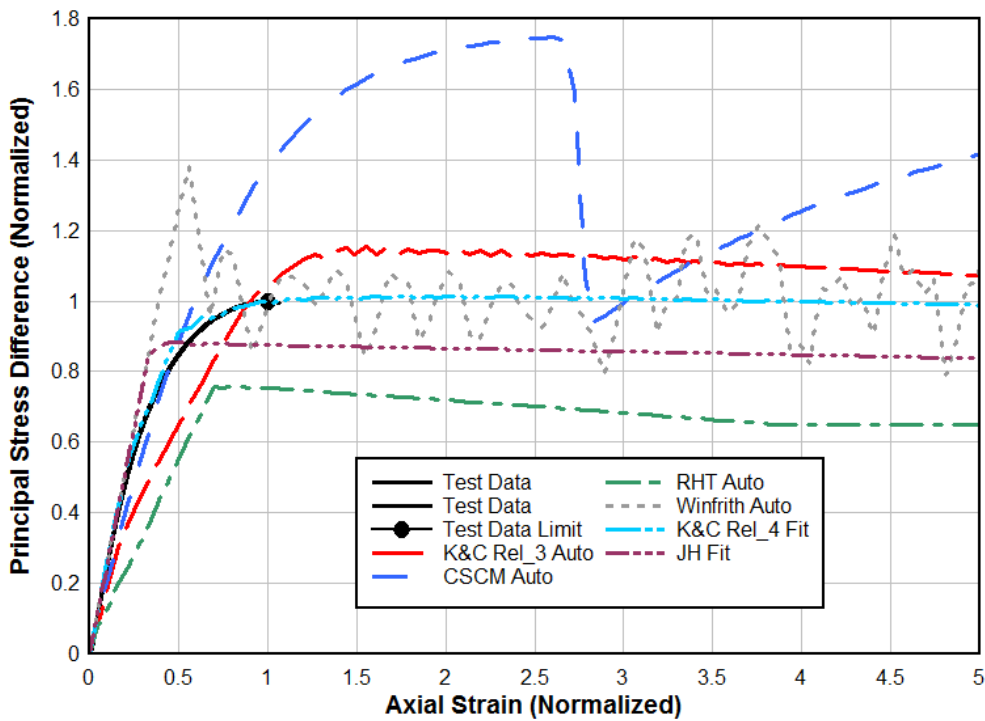


Figure 5: Triaxial Compression with 1x Confining Pressure Material Test vs. Simulation Results

Triaxial Compression with 4x Confining Pressure

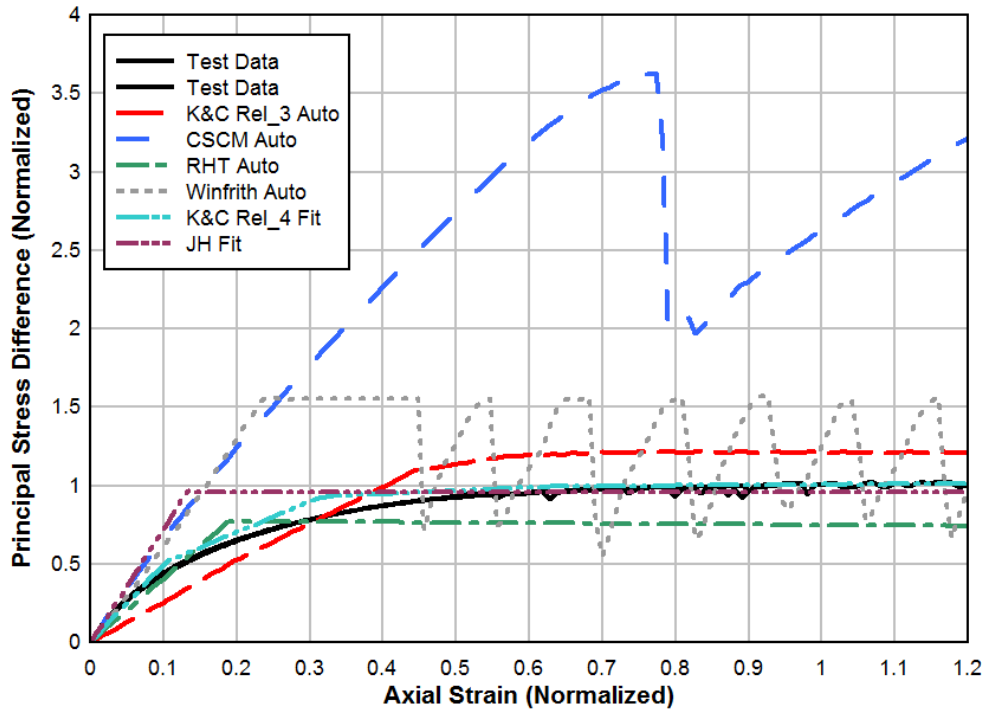


Figure 6: Triaxial Compression with 4x Confining Pressure Material Test vs. Simulation Results (Complete)

Triaxial Compression with 4x Confining Pressure

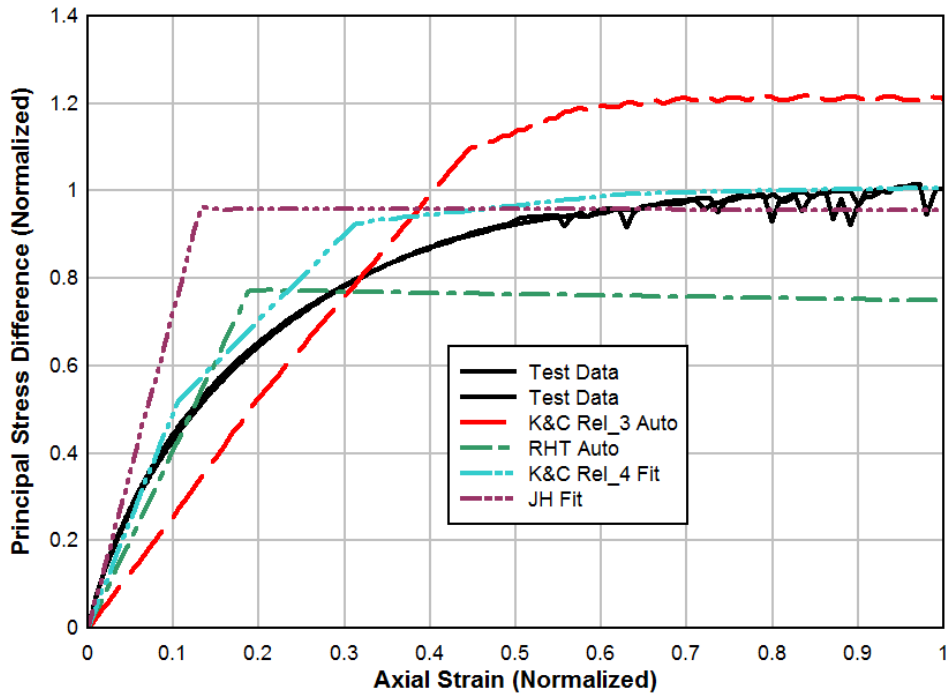


Figure 7: Triaxial Compression with 4x Confining Pressure Material Test vs. Simulation Results (Partial)

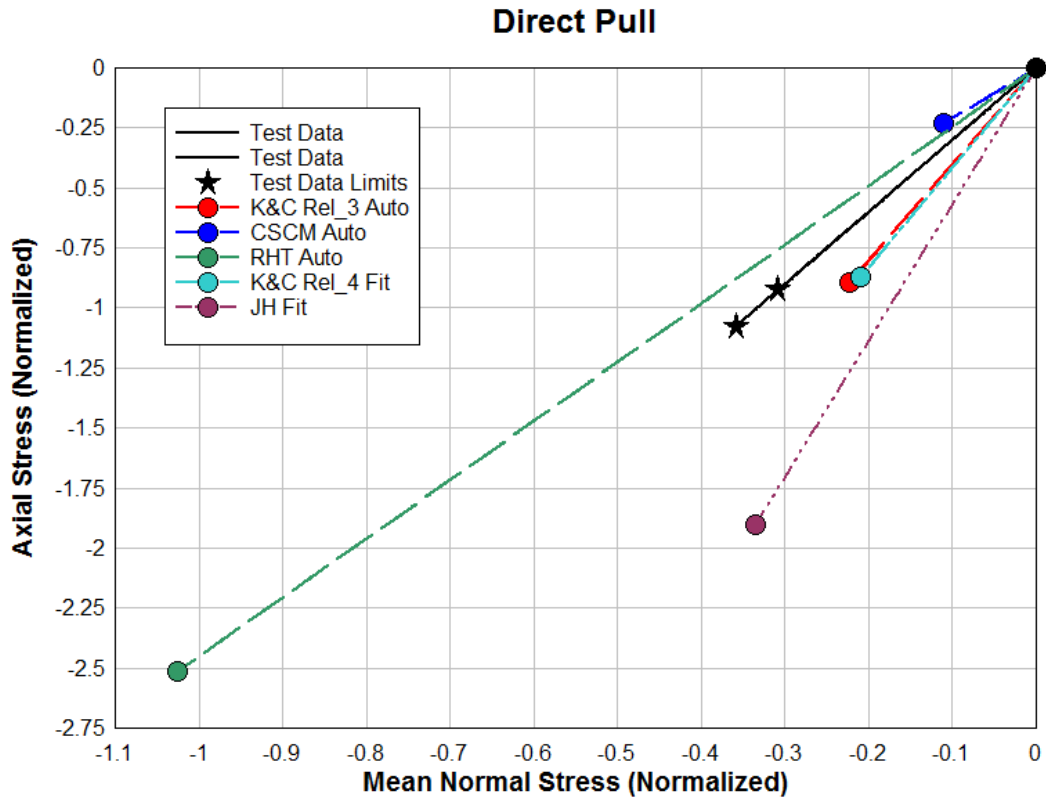


Figure 8: Direct Pull Material Test vs. Simulation Results

Impact Simulations

Impact simulations were also conducted using LS-DYNA to determine the ability of each concrete material model to reproduce the slab response observed during testing. Because the tests involved projectile impact normal to the slab, quarter-symmetry geometry of the test target and projectile were utilized to reduce the computational cost as shown in Figure 9. While the geometry of the projectile is not displayed, the concrete response is shown to provide qualitative information for each simulation. For each concrete material model, one case was simulated for each of the two experimental impact tests (Test 1 and Test 2) and compared against the other material models. Because Test 1 and Test 2 did not use identical reinforced concrete slab configurations, it is expected that the simulation results should be different for each test, even though the same projectile and same concrete material is used.

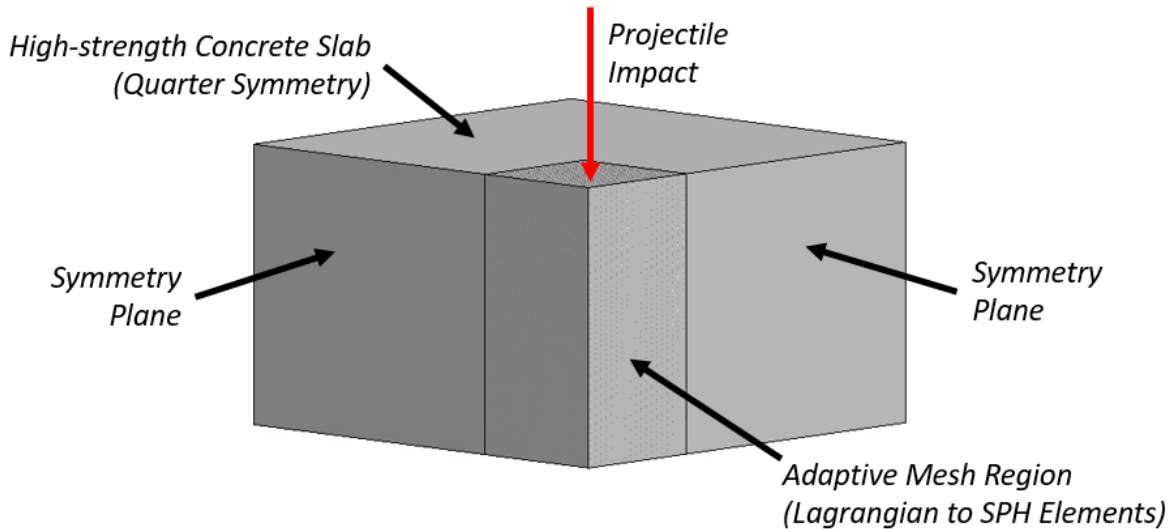


Figure 9: LS-DYNA Impact Model Setup

Simulation of high-velocity impact problems involving concrete often requires erosion of solid Lagrangian elements to avoid extreme element distortion leading to very small time steps or negative element volumes. The authors elected to take this approach based on the positive results seen in similar previous computations. In order to conserve the mass and resistance of the slab as much as possible, the solid elements were converted to smoothed particle hydrodynamics (SPH) elements once a failure strain criterion was reached. Because SPH elements are not subject to heavy distortion or negative volumes as solid elements are, the conversion of elements in critical regions allowed the computation to continue progressing steadily without the removal of any mass from the problem. By utilizing primarily solid elements throughout the duration of the simulation, the model is not subjected to the computational cost of using all SPH elements or the greater potential for tensile instabilities which are specific to the SPH formulation. This balanced approach of converting solid elements to SPH elements only in regions of large tensile strains has proven to be effective for problems involving impact and penetration into concrete.

The simulation results show a range of penetration depths and exit velocities across the various concrete material models under investigation. Figures are provided at the end of each test section displaying the simulation results plotted against the experimental data. As the test data did not include penetration-time histories as produced by the simulations, the reference experimental values are simply the final depth of penetration or exit velocity of the projectile. In the comparison plots, the depth of penetration is normalized to the depth of the slab, and the projectile velocity is normalized to the impact velocity of the projectile. The following two items were of critical interest during the evaluation of the projectile impact simulation results:

- Determination of whether the use of automatic parameter generation for concrete material models is generally reliable for the specific class of projectile impact problems being investigated
- Correlations between high-strength concrete model fits to quasi-static material test data and the ability to reproduce the concrete response to projectile impact

Test 1 Impact Simulations

K&C Release 3 with Automatic Parameter Generation

The simulation using the K&C Release 3 model with automatic parameter generation results in a depth of penetration which is equal to 56% of the slab depth, whereas the experimental test resulted in perforation with a low exit velocity. Thus, the model predicts a much stiffer slab response than that which was observed in the test. This may be the result of the parameter generation feature over-estimating the concrete strength at elevated confining pressures or producing values for the dilatancy or damage evolution which are not consistent with the actual material properties.

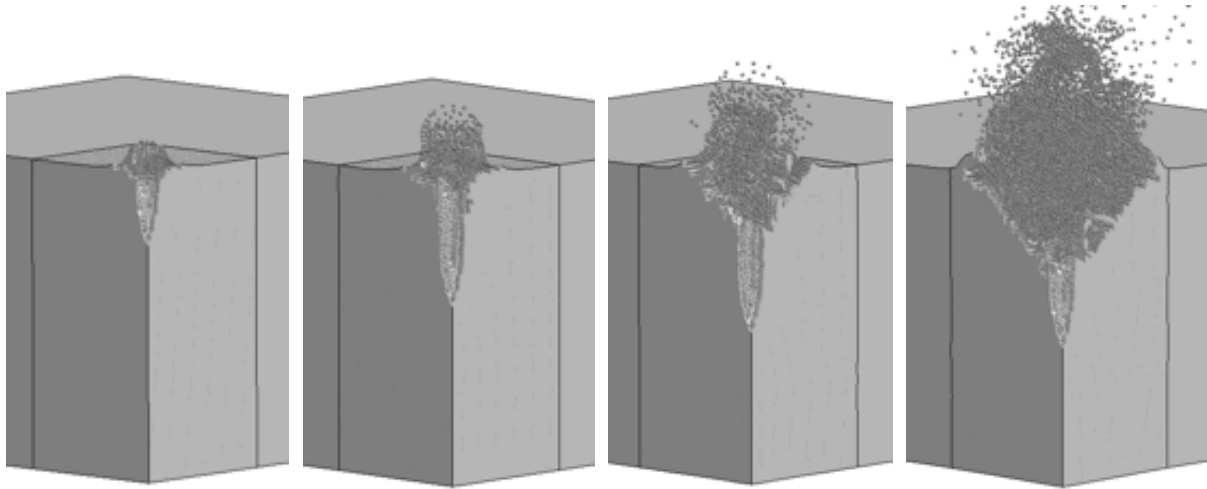


Figure 10: Simulation Test 1 Progression of Concrete Penetration – K&C Release 3

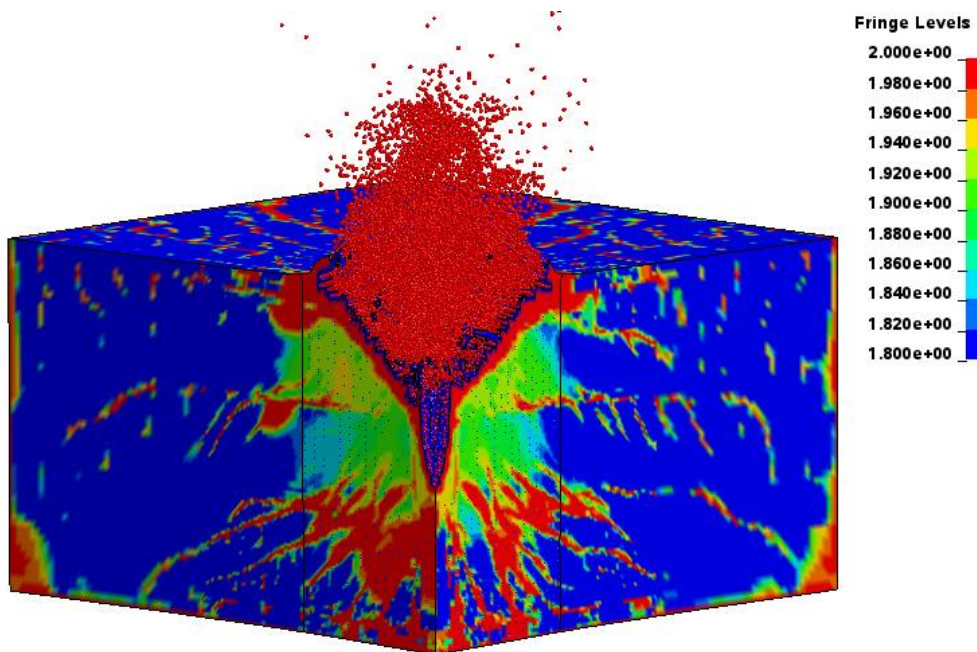


Figure 11: Simulation Test 1 K&C Release 3 Contours of Damage

CSCM with Automatic Parameter Generation

The simulation using the CSCM model with automatic parameter generation results in a slab perforation with an exit velocity equal to 58% of the impact velocity. Thus, the model significantly under-predicts the resistance of the slab. It is important to note that the CSCM automatic generation default concrete input parameters are for normal strength concrete with unconfined compression strengths between about 28 and 58 MPa (Livermore Software Technology Corporation 2015), but the concrete under investigation has a strength above this range. However, the model will still accept strength values outside of the “normal” strength range, and the simulation completed without any instabilities. The authors determined that the simulations were still a valuable component of the study given that software users

will push the limits of the automatic generation feature for the sake of convenience and time. In this case, the results provide a clear warning against this mindset.

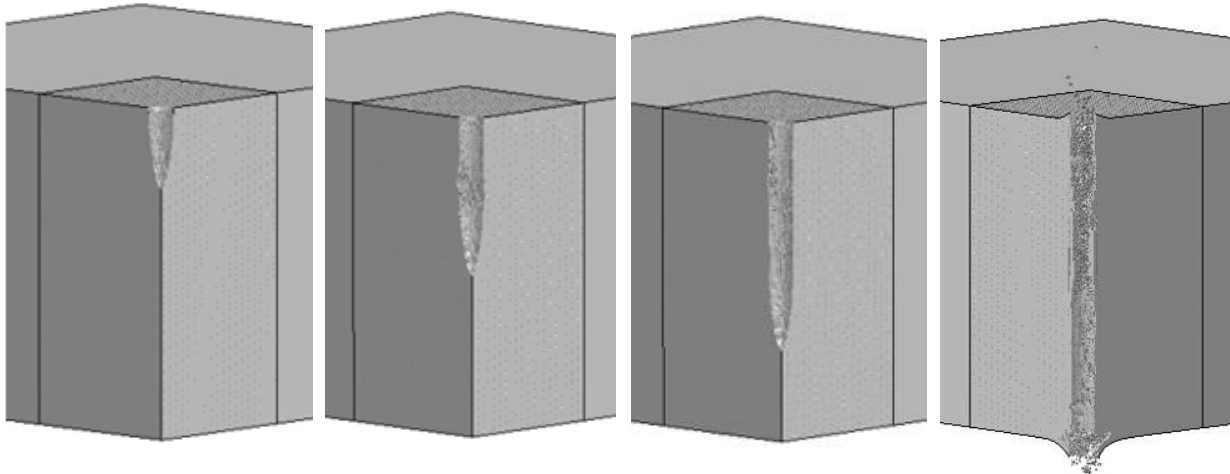


Figure 12: Simulation Test 1 Progression of Concrete Penetration – CSCM

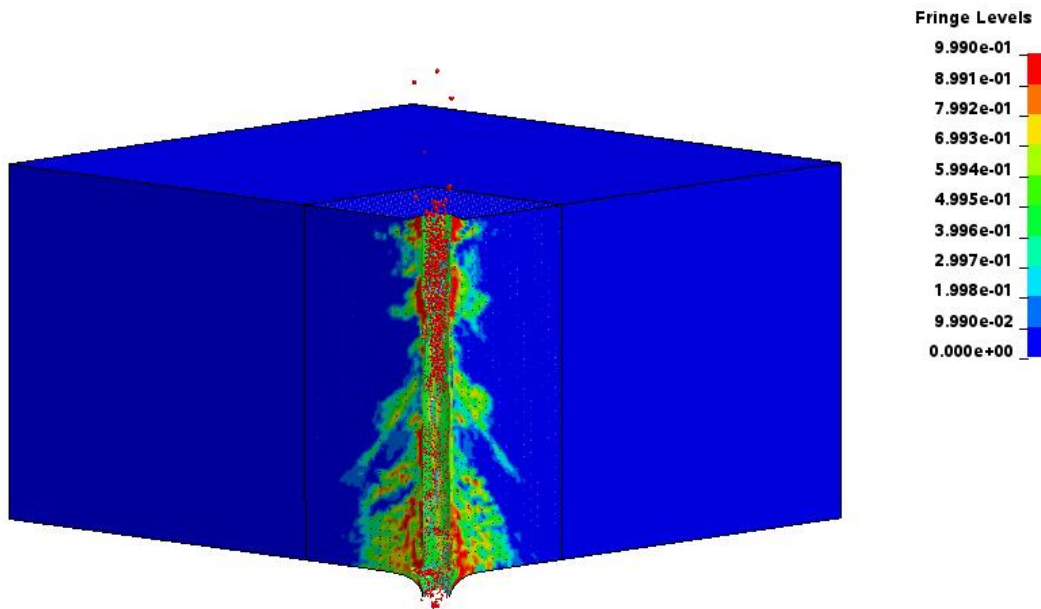


Figure 13: Simulation Test 1 CSCM Contours of Damage

RHT with Automatic Parameter Generation

The RHT impact simulation was unable to run to completion due to a computer memory error which repeatedly occurred with multiple attempts. Thus, the images below show the simulation results up to the point of the error, but the simulated final depth of penetration should be greater than that being displayed. This is made evident by the plots in Figure 20 and Figure 21. If the final simulation result is estimated based on the trend of the projectile displacement and velocity curves, the model does a much better job reproducing the test result than any of the other models using automatic parameter generation. In fact, the match between the projectile displacement-time history for the RHT model and K&C Release 4 model up to the point of the error is nearly exact. Given that the K&C Release 4 model

produced an exit velocity which was within a few percent of the normalized test result, this provides some indication that the RHT would also likely produce a reasonable result in the absence of the memory error.

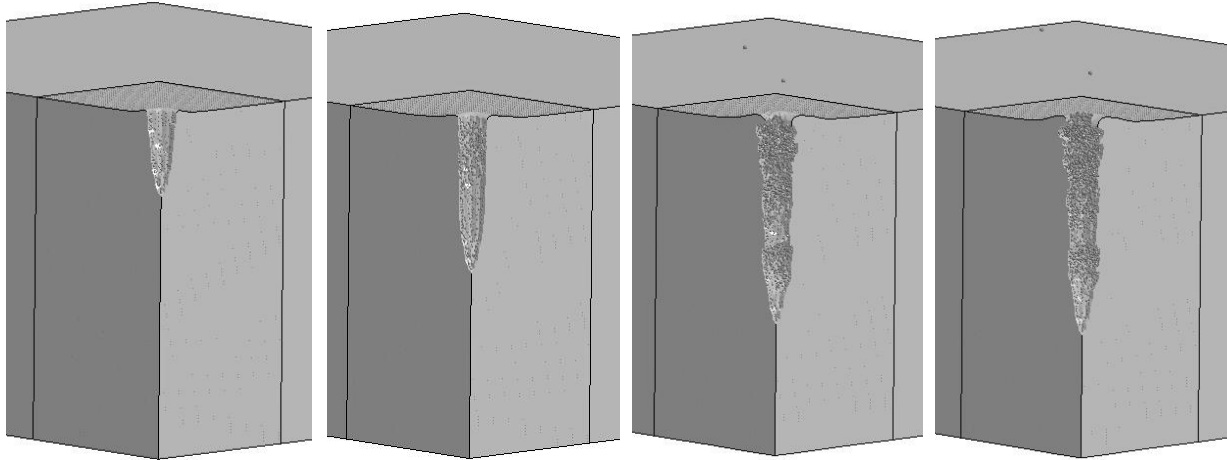


Figure 14: Simulation Test 1 Progression of Concrete Penetration - RHT

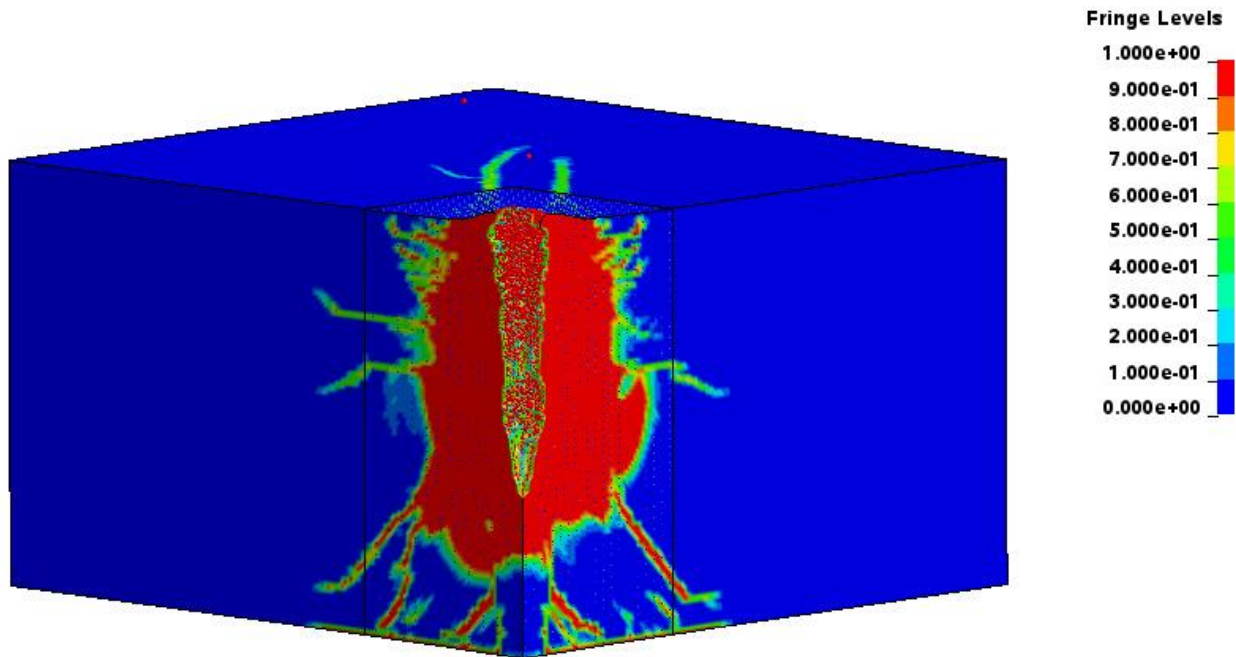


Figure 15: Simulation Test 1 RHT Contours of Damage

Johnson-Holmquist Fit to Material Test Data

The Johnson-Holmquist model over-predicts the resistance of the slab, with the final depth of penetration being equal to 69% of the slab depth. The model performs better than the CSCM or K&C Release 3 models with automatic parameter generation but worse than the K&C Release 4 model which was fit to the material test data.

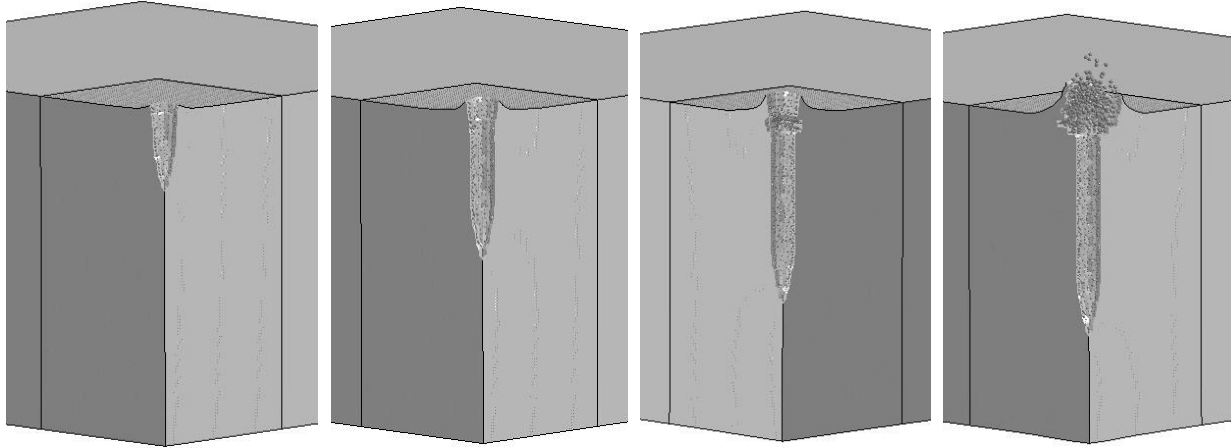


Figure 16: Simulation Test 1 Progression of Concrete Penetration – Johnson Holmquist

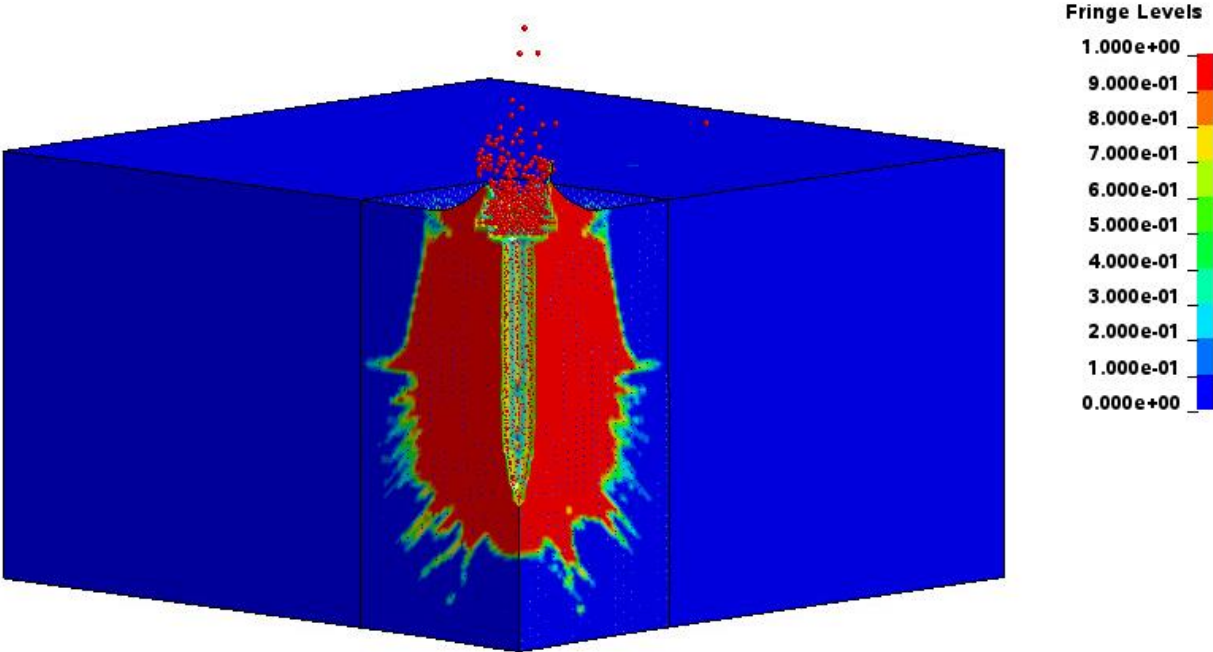


Figure 17: Simulation Test 1 Johnson-Holmquist Contours of Damage

K&C Release 4 Fit to Material Test Data

The K&C Release 4 model reproduces the test result with reasonable accuracy, resulting in an exit velocity which is 14% of the impact velocity, compared to the experimental result of 6% of the impact velocity.

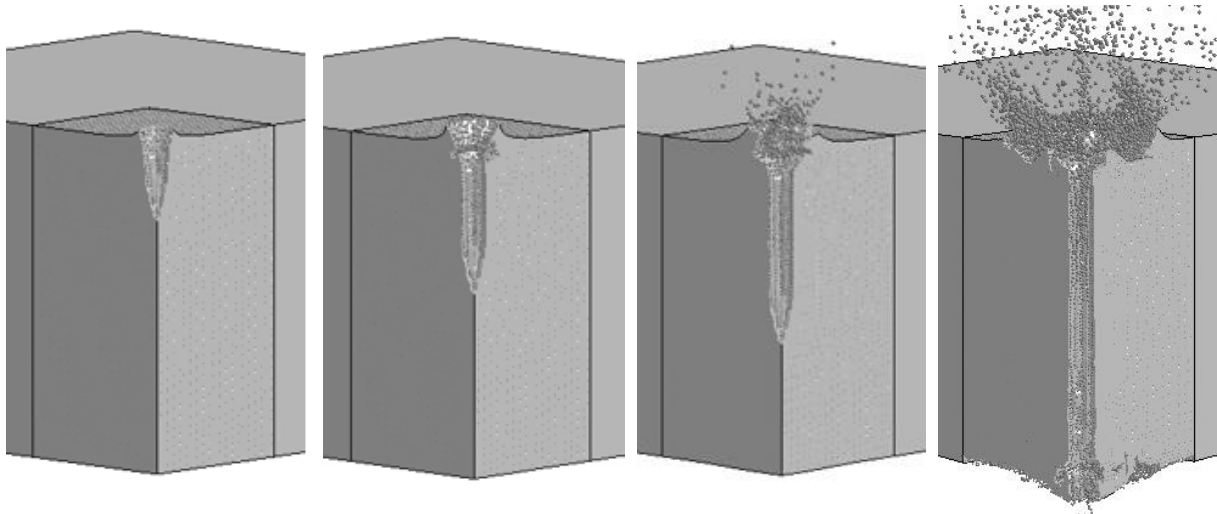


Figure 18: Simulation Test 1 Progression of Concrete Penetration – K&C Release 4

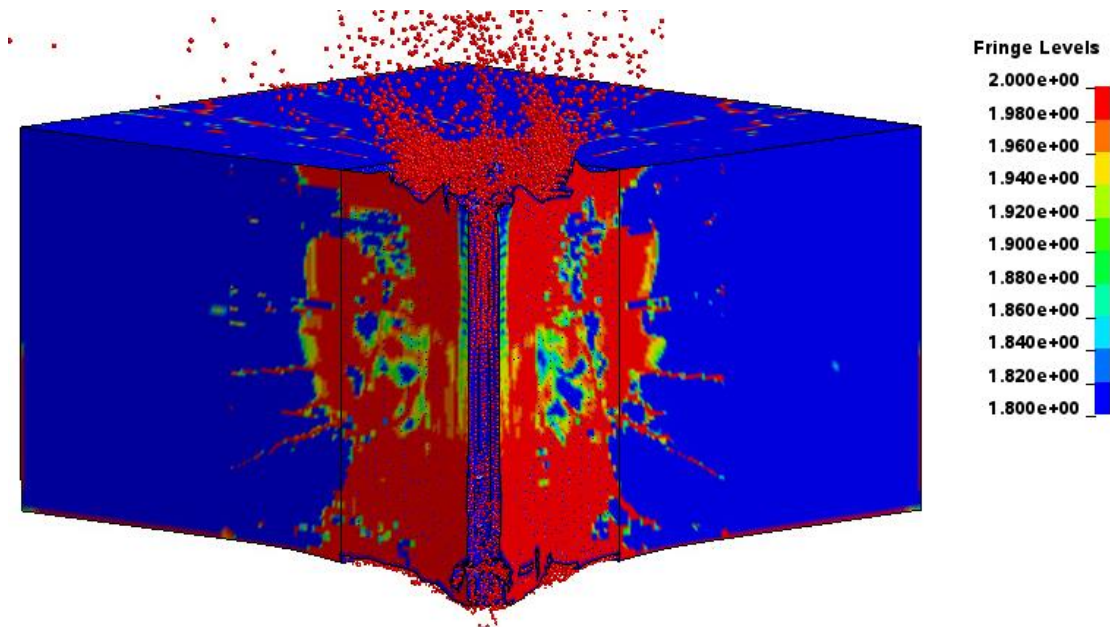


Figure 19: Simulation Test 1 K&C Release 4 Contours of Damage

Simulations vs. Experimental Results Test 1 - Displacement

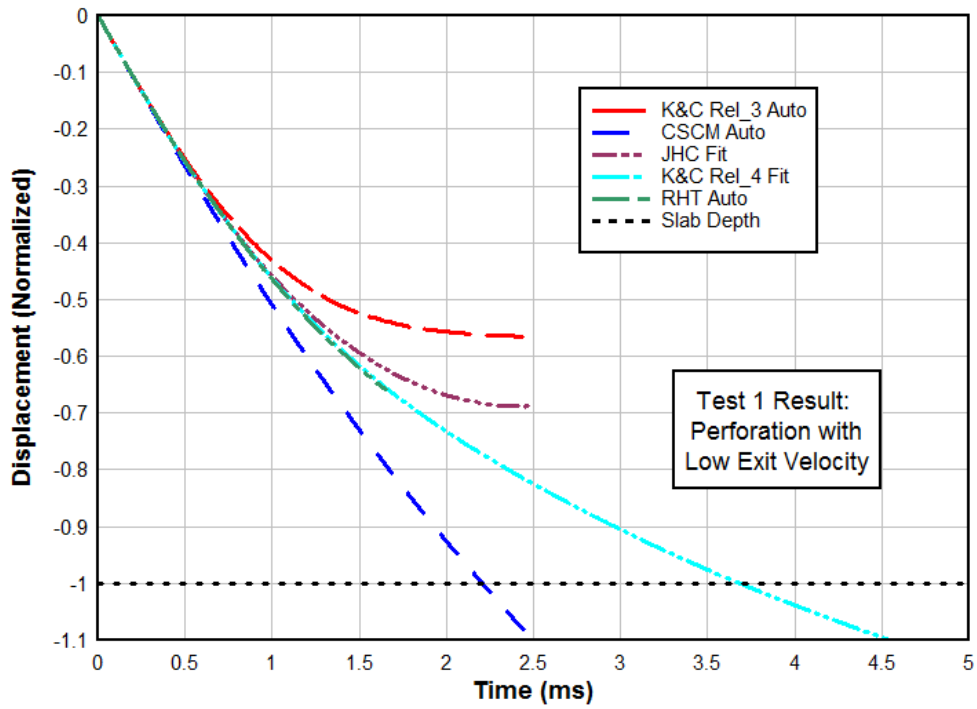


Figure 20: Simulations vs. Experimental Results for Test 1 Projectile Displacement

Simulations vs. Experimental Results Test 1 - Velocity

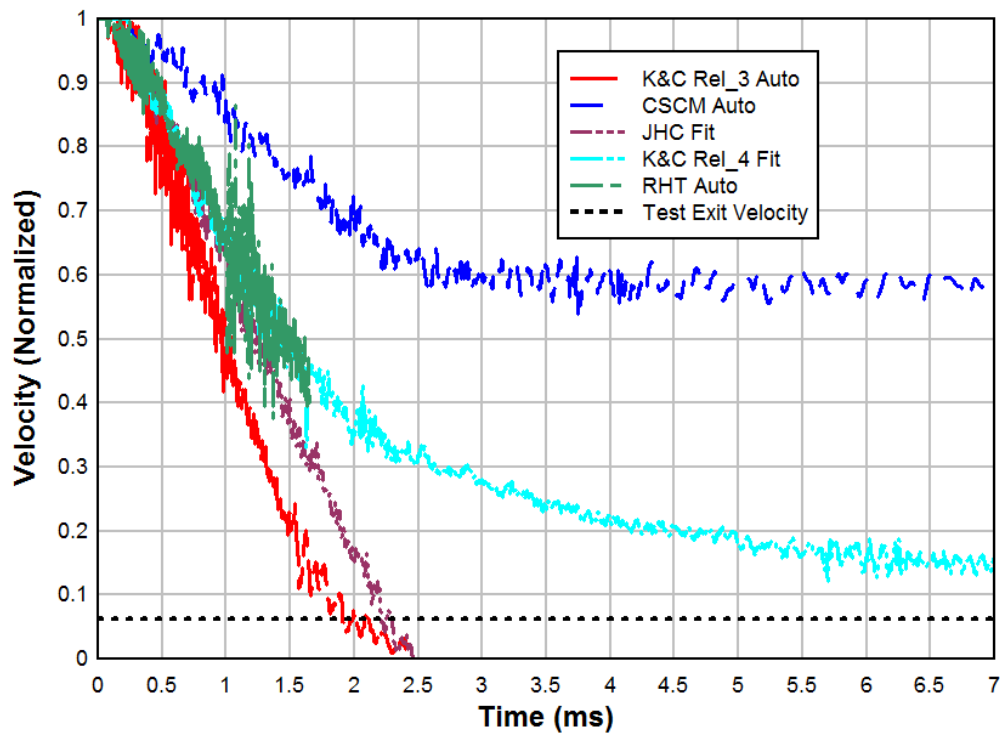


Figure 21: Simulations vs. Experimental Results for Test 1 Projectile Velocity

Test 2 Impact Simulations

K&C Release 3 Auto

The simulation using the K&C Release 3 model with automatic parameter generation results in a DOP which is equal to 46% of the slab depth compared to the experimental result of 97% of the slab depth. Thus, the model predicts a much stiffer slab response than that which was observed in the test. As noted previously, this may be the result of the parameter generation feature over-estimating the concrete strength at elevated confining pressures or producing an unrealistic value for another generated parameter such as the dilatancy. For this model as well as all other Test 2 models, the damage observed at the upper surface of the slab is the result of an additional boundary element in both the test setup and simulation which is not present in Test 1. The details of this item are intentionally excluded from this study.

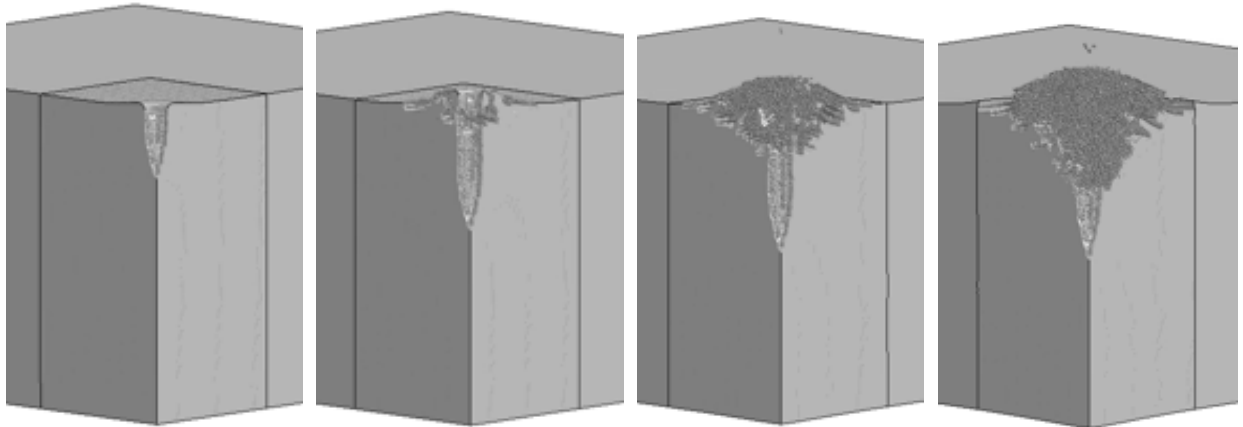


Figure 22: Simulation Test 2 Progression of Concrete Penetration – K&C Release 3

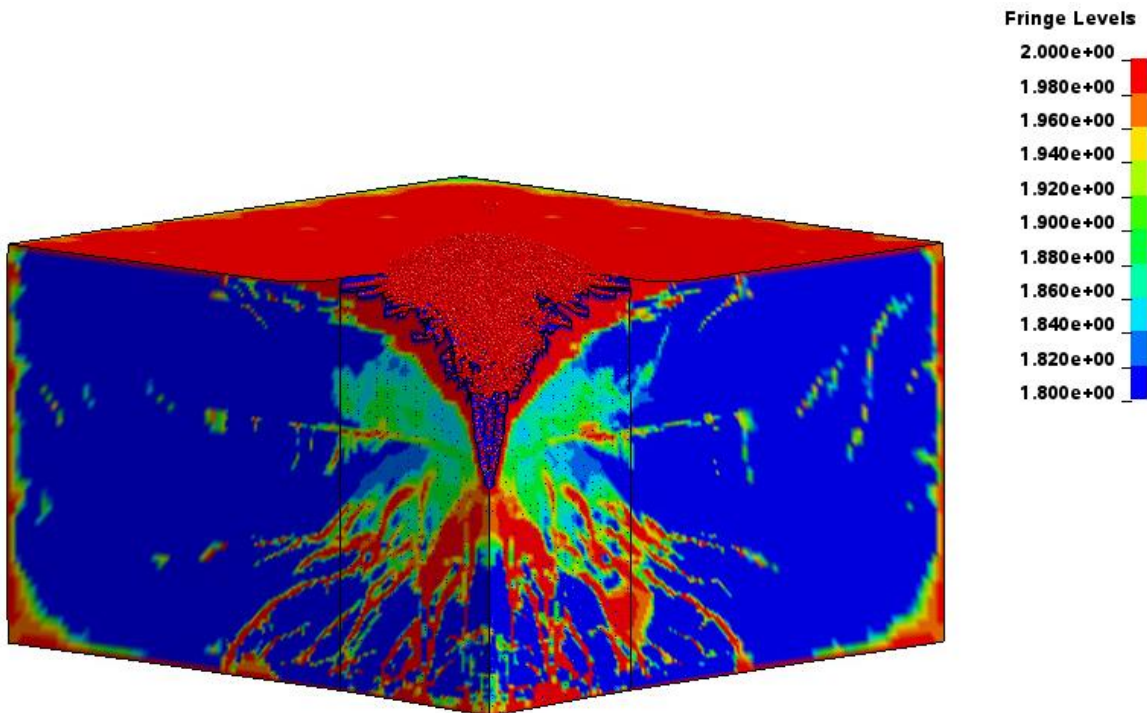


Figure 23: Simulation Test 2 K&C Release 3 Contours of Damage

CSCM with Automatic Parameter Generation

The CSCM model significantly underestimates the resistance of the slab, producing a projectile exit velocity which is equal to 45% of the impact velocity, whereas perforation was fully resisted in the test. The likely cause of this simulation result are discussed in the Test 1 section.

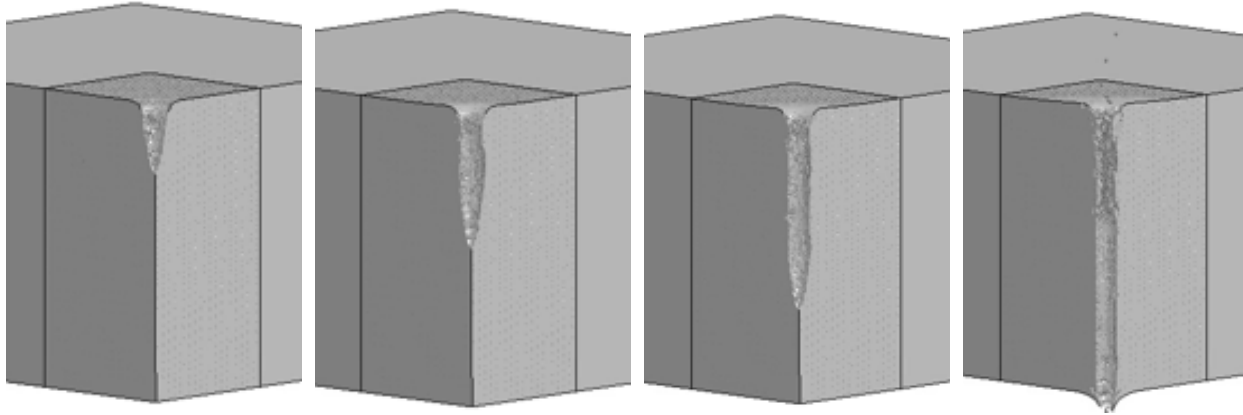


Figure 24: Simulation Test 2 Progression of Concrete Penetration - CSCM

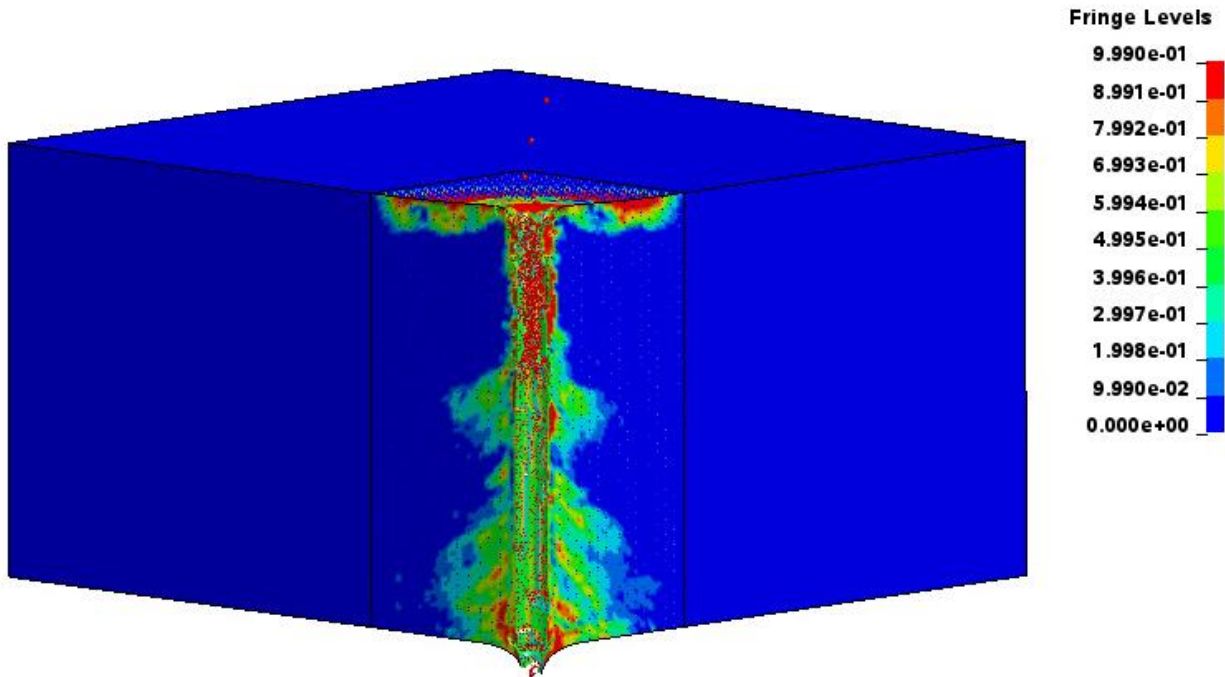


Figure 25: Simulation Test 2 CSCM Contours of Damage

RHT with Automatic Parameter Generation

As previously noted, the RHT impact simulation was unable to run to completion due to a computer memory error which repeatedly occurred with multiple attempts. Similar to Test 1, the simulation results show that the model would likely outperform all other models with the exception of K&C Release 4 in the absence of the memory error causing premature termination.

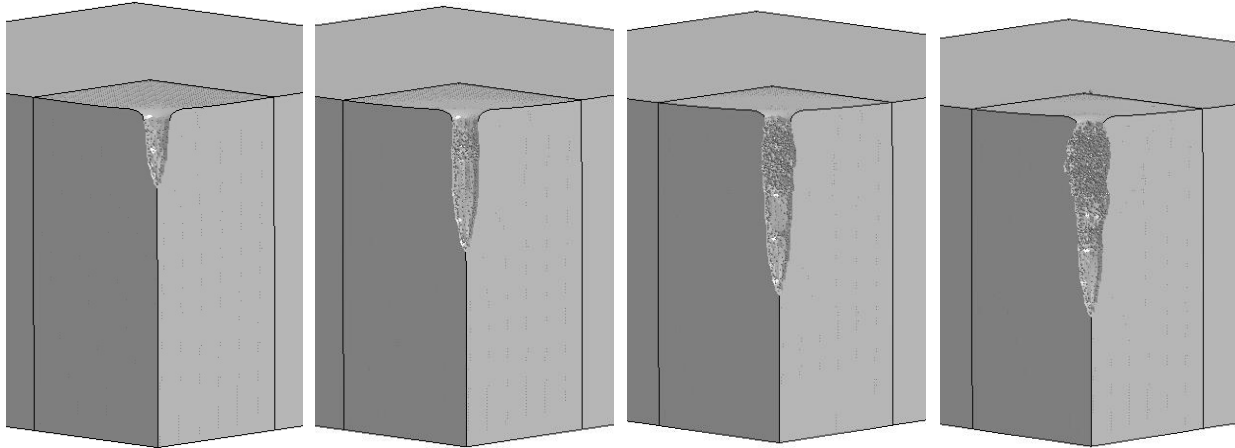


Figure 26: Simulation Test 2 Progression of Concrete Penetration - RHT

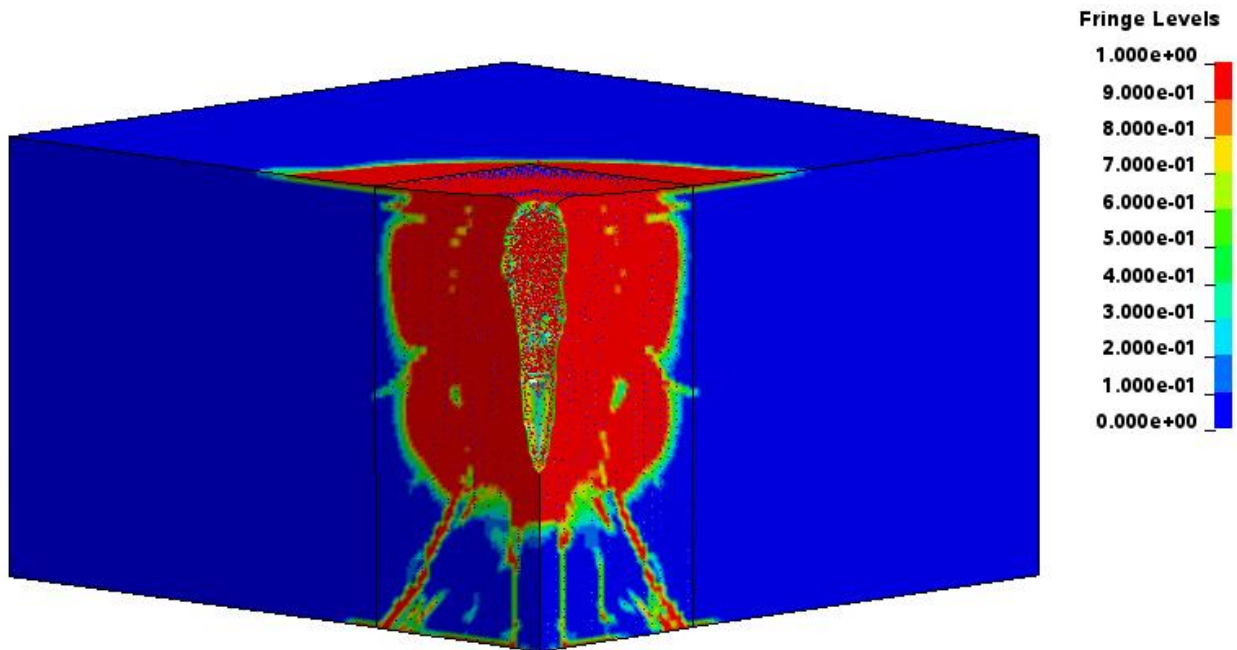


Figure 27: Simulation Test 2 RHT Contours of Damage

Johnson-Holmquist Fit to Material Test Data

Similar to the Test 1 simulation, the Johnson-Holmquist model over-predicts the resistance of the slab, with the final depth of penetration being equal to 57% of the slab depth compared to the test result of 97%. The model performed better than the CSCM or K&C Release 3 models with automatic parameter generation but worse than the K&C Release 4 model which was fit to the material test data.

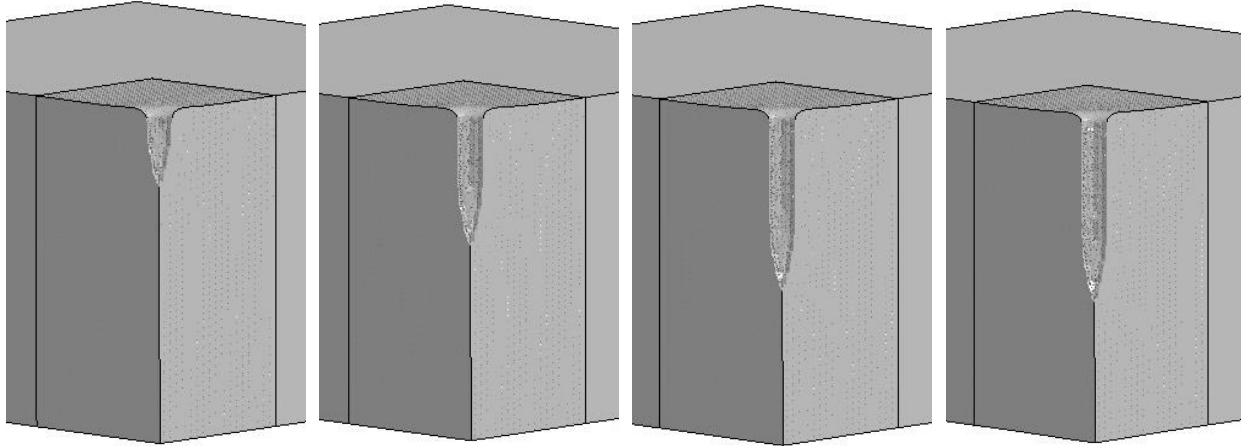


Figure 28: Simulation Test 2 Progression of Concrete Penetration – Johnson-Holmquist

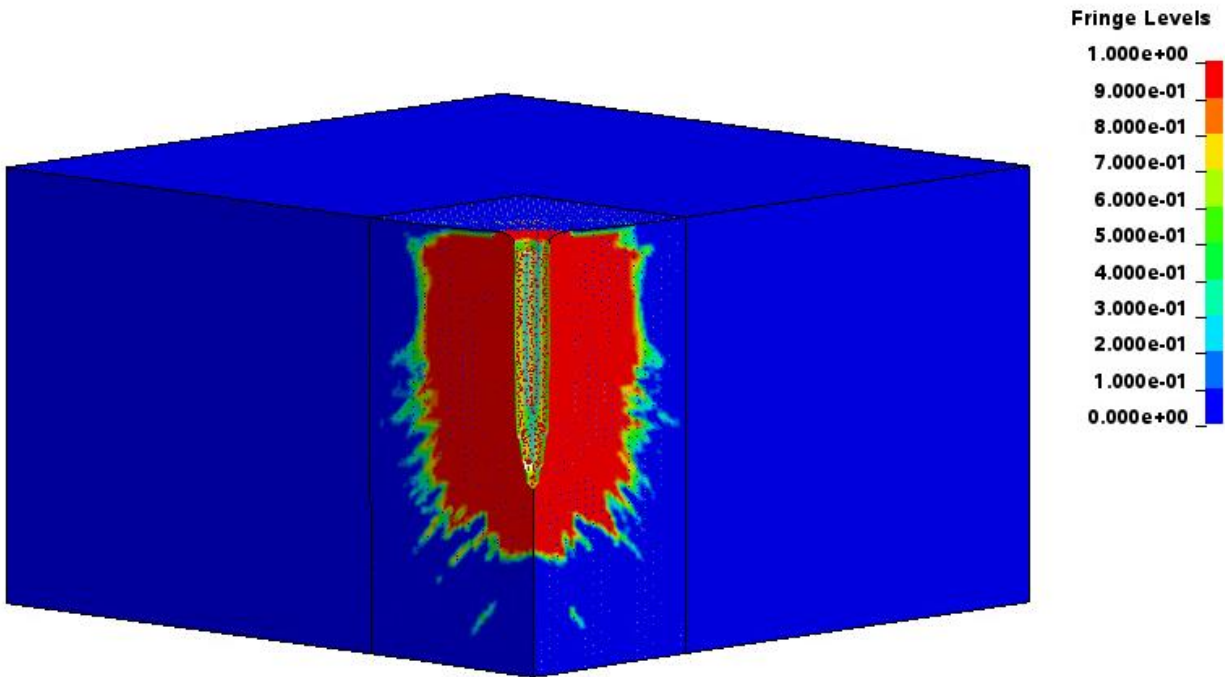


Figure 29: Simulation Test 2 Johnson-Holmquist Contours of Damage

K&C Release 4 Fit to Material Test Data

The K&C Release 4 model reproduces the test result with reasonable accuracy, resulting in a depth of penetration which is equal to 85% of the slab depth, compared to the experimental result of 97%.

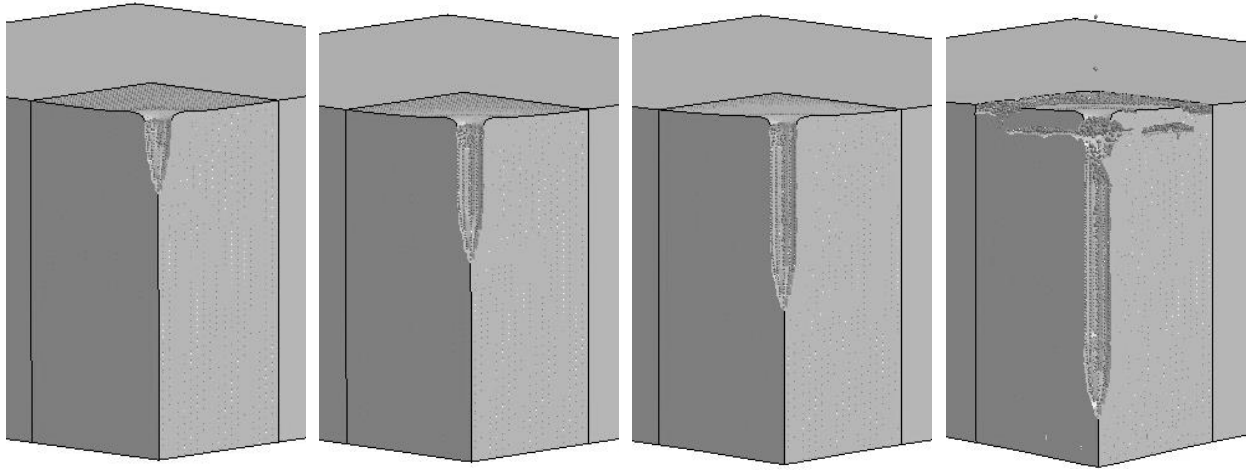


Figure 30: Simulation Test 2 Progression of Concrete Penetration – K&C Release 4

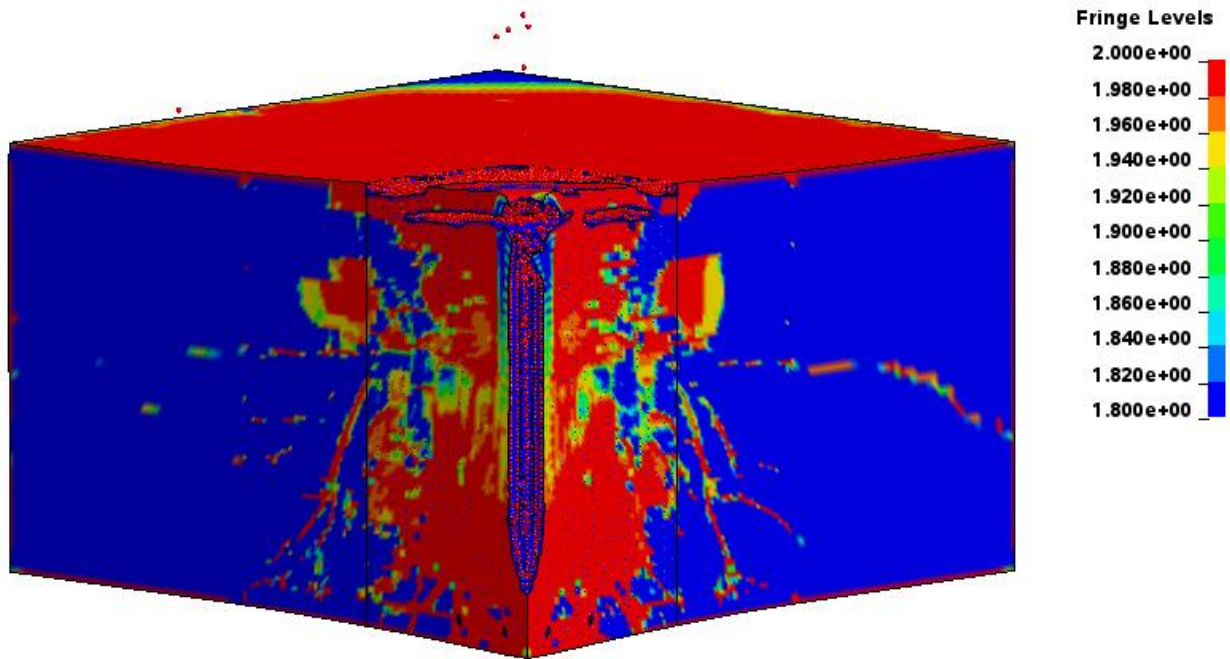


Figure 31: Simulation Test 2 K&C Release 4 Contours of Damage

Simulations vs. Experimental Results Test 2 Displacement

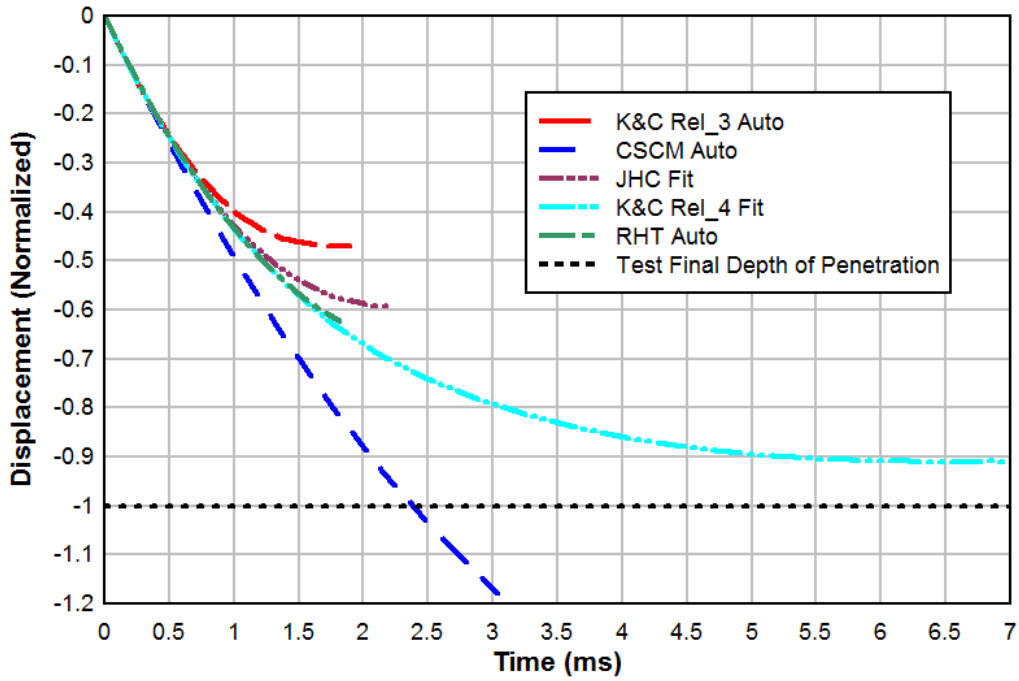


Figure 32: Simulations vs. Experimental Results for Test 2 Projectile Displacement

Simulations vs. Experimental Results Test 2 - Velocity

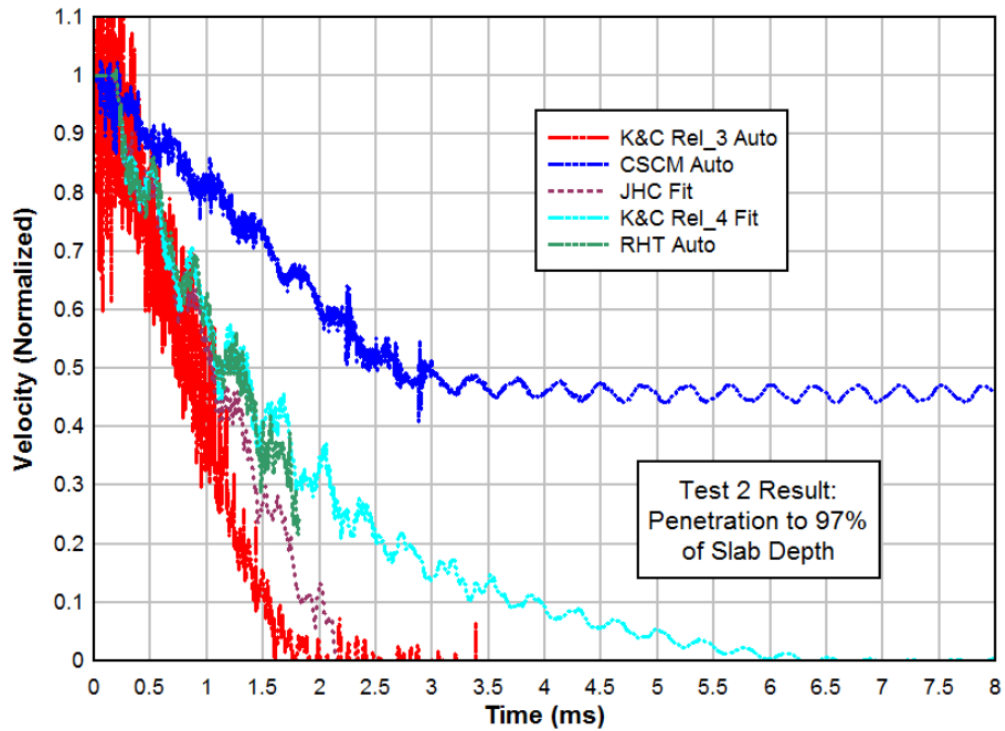


Figure 33: Simulations vs. Experimental Results for Test 2 Projectile Velocity

Table 3: Summary of Simulation Results vs. Experimental Results

Test	Material Model	Simulation Result (DOP / Slab Depth or Exit Velocity / Impact Velocity)*	Experimental Result (DOP / Slab Depth or Exit Velocity / Impact Velocity)*
1	K&C Rel. 3 Auto	DOP/DS = 0.56	VE/VI = 0.06
	CSCM Auto	VE/VI = 0.58	
	RHT Auto	VE/VI \approx 0 – 0.20 **	
	JHC Fit	DOP/DS = 0.69	
	K&C Rel. 4 Fit	VE/VI = 0.14	
2	K&C Rel. 3 Auto	DOP/DS = 0.46	DOP/DS = 0.97
	CSCM Auto	VE/VI = 0.45	
	RHT Auto	DOP/DS \approx 0.70 – 0.80 **	
	JHC Fit	DOP/DS = 0.57	
	K&C Rel. 4 Fit	DOP/DS = 0.85	

* VE = Exit Velocity; VI = Impact Velocity; DOP = Depth of Penetration; DS = Slab Depth

** Range estimated based on observed trends in simulation results up to point of memory error

Conclusions

Several concrete material models were evaluated using LS-DYNA to determine their ability to reproduce the results observed during experimental impact testing with a generic projectile. The results show that users should exercise extreme caution when considering the use of automatically generated material parameters for problems involving projectile impact into high-strength concrete. All of the concrete models evaluated in this study with this parameter generation feature were unable to reproduce the experimental impact results, even when reasonable fits to the quasi-static test data were observed. The complexity of impact events demands that analysts take the extra steps to ensure the validity of concrete models for the specific scenario under examination. In most cases, this will require a custom fit to material test data and individual input of all required parameters.

A few observations regarding comparisons between the quasi-static material test data fits and impact simulation results for each model are worth noting. The K&C Release 4 model was fit to the quasi-static test data better than any other model and also produced the best results in the impact simulations. The CSCM model’s automatic generation feature significantly over-estimated the material strength at both the 1x and 4x confining pressures, which was an indication that the tool may have been operating outside of its intended bounds as also noted in the literature (Livermore Software Technology Corporation 2015). The poor results observed in the impact simulations are not surprising. Of all the models using automatic parameter generation, the RHT model produced the best overall results for both the quasi-static and impact simulations. This conclusion of course assumes that the memory error issue can be resolved and that the model will run to completion. In general, better fits to material test data will result in a better ability to simulate impact of projectiles into concrete.

The study also shows that high-fidelity physics-based software tools are capable of accurately simulating impact and penetration into reinforced concrete protective construction features when care is taken by the analyst to properly model the material. The K&C Release 4 model was fit to the quasi-static material test data and subsequently able to reproduce the results of both impact tests with reasonable accuracy. Although the approach requires more time and computer resources than other methods, it provides the ability to model complex loading scenarios and produces a much higher level of detail in terms of structural response and the associated hazards. While these computations are not currently the common or preferred practice for projects involving explosives safety and UFC 3-340-02 compliance, engineers should continue to pursue the development of these approaches with an eye towards rigorous validation of models and clear documentation of the value provided by these simulations. Explosives storage and operating locations will be better supported when more accurate solutions for complex loading scenarios such as debris impact can be provided through high-fidelity analysis.

References

- DoD 6055.09M. 2010. "DoD Ammunition and Explosives Safety Standards: General Explosives Safety Information and Requirements."
- DoD. 2014. "Unified Facilities Criteria 3-340-02: Structure to Resist the Effects of Accidental Explosions." UFC 3-340-02.
- Magallanes, Joseph M. 2008. "Importance of concrete material characterization and modeling to predicting the response of structures to shock and impact loading." In *Structures Under Shock and Impact X*. Southampton: WIT Press.
- Wu, Youcai, John E Crawford, and Joseph M Magallanes. 2012. "Performance of LS-DYNA Concrete Constitutive Models." *12th LS-DYNA User's Conference*. Dearborn, MI.
- Crawford, John E, Youcai Wu, Joseph M Magallanes, and Hyung Jin Choi. 2013. "The Importance of Shear-Dilatancy Behaviors in RC Columns." *Int. J. Prot. Struct.* 4 (3): 341-377.
- Wu, Youcai, John E Crawford, Shengrui Lan, and Joseph M Magallanes. 2014. "Validation of concrete constitutive models through blast responses." *13th LS-DYNA International Conference*. Dearborn, MI.
- Coleman, Daniel. 2016. "Evaluation of Concrete Modeling in LS-DYNA for Seismic Application." Master's Thesis, Austin, TX.
- Malvar, L. J., Crawford, J. E., Wesevich, J. W., Simons, D. 1997. "A Plasticity Concrete Material Model for DYNA3D." *International Journal of Impact Engineering*, vol. 19, no. 9/10, 847-873.
- Chen, W F. 1982. *Plasticity in Reinforced Concrete*. New York: McGraw Hill.
- Crawford, J. E., Wu, Y., Choi, H. J., Magallanes, J. M., Lan, S. 2011. "Use and Validation of the Release III K&C Concrete Material Model in LS-DYNA." Technical Report TR-11-36.5, Glendale, CA.
- Federal Highway Administration, USA. May 2007. "User Manual for LS-DYNA Concrete Material."
- Brannon, R. M. and Leelavanichkul, S. August 2009. *Survey of Four Damage Models for Concrete*. SAND2009-5544, Albuquerque, NM: Sandia National Laboratories.
- Borrvall, T., and W. Riedel. May 2011. "The RHT Concrete Model in LS-DYNA." *8th European LS-DYNA Users Conference*. Strasbourg.
- Ottosen, N.S. 1977. "A Failure Criterion for Concrete." *Journal of the Engineering Mechanics* 527-535.
- Broadhouse, B.J. 1995. "The Winfrith Concrete Model in LS-DYNA3D."
- Holmquist, T. J., and G. R. Johnson. 1993. "A Computation Constitutive Model for Contract Subjected to Large Strains, High Strain Rates, and High Pressures." *International Symposium on Ballistics*. 591-600.
- Livermore Software Technology Corporation, LSTC. 2015. "LS-DYNA Keyword User's Manual." Livermore, CA.
- Butenweg, Christoph, Anne Kleemann, Okyay Altay, and Philippe Renault. 2013. "Simulation of Impact-Loads on Reinforced Concrete Structural Elements." *22nd Conference on Structural Mechanics in Reactor Technology*. San Francisco, CA.
- Grunwald, Christoph, Benjamin Schaufelberger, Alexander Stolz, Werner Riedel, and Thomas Borrvall. 2017. "A General Concrete Model in Hydrocodes: Verification and Validation of the Riedel-Hiermaier-Thoma Model in LS-DYNA." *International Journal of Protective Structures* Vol. 8 pp. 58-85.
- Schwer, Len. 2010. *An Introduction to the Winfrith Concrete Model*. Schwer Engineering and Consulting Services.
- Schwer, Leonard E., and Yvonne D Murray. 2007. "Continuous Surface Cap Model for Geomaterial Modeling: A New LS-DYNA Material Type." *7th International LS-DYNA Users Conference*. 35-50.
- Winkelbauer, Bradley J. 2015. *Phase I Evaluation of Selected Concrete Material Models in LS-DYNA*. Master's Thesis, Lincoln, Nebraska: University of Nebraska Dept. of Civil Engineering.